University of Freiburg

Synthesis and characterization of Semiconducting Nano-Particles for Water-Processable Active Layers for OLEDs

Master's Thesis Project – Presented to the Faculty of Chemistry and Pharmacy at Albert-Ludwig's University of Freiburg

In Partial fulfilment
of the requirements for the degree of

Master of Science – Sustainable Materials – Polymer Science (binational)

Submitted by: Ahmed Fakih
Matriculation Number: 4560187

Research work carried out at: Max Planck Institute for Polymer Research, Mainz

MAX PLANCK INSTITUTE
FOR POLYMER RESEARCH

Supervisors
University of Freiburg: Prof. Dr. Rolf Mülhaupt
MPIP: Dr. Jaspers Michels, Anielen Halda Ribeiro

Abstract

Semi-conducting polymers, which have applications in organic electronic devices such as OLEDs and OPVs, have an important hindering effect, which is the presence of electronic charge traps which influence the charge transport and can reduce the performance of polymers based electronic devices. As reported by Blom et. Al [2], the effect of these traps can be diluted by blending of a semi-conducting polymer with an insulating polymer. Secondly, the advantage of use of polymers for devices such as OLEDs is the ability to be processed from solutions. Currently, the solution-based process uses organic and halogenated solvents to fabricate layers for OLEDs. In order to improve the process to make it greener, water has been touted as possible a desirable solvent for film fabrication. However, as most of the semi-conducting polymers are hydrophobic, direct processing of films based of polymers via water as a solvent is not feasible. The blending of two polymers provides a challenge as well as polymers usually display low miscibility with each other, tend to phase separate in films. Both of these challenges of phase separation and synthesizing active layers for OLEDs from environmentally friendly solvent was addressed by confining a polymer blend within a nanoparticle dispersed in water. The nanoparticles are synthesized using mini-emulsion method[3]and the polymers blended in different weight ratios of semi-conductor to insulator polymers to observe the effect of trap dilution. In this thesis project, three different blended systems of polymers were utilized namely Super-Yellow PPV/Polystyrene, MEH-PPV/Polystyrene, PFO/Polystyrene. For all three systems, three different blend weight ratios of 1:1, 1:3, 1:5 of semi-conductor: insulator was applied for nanoparticles. The blend morphology within the nanoparticle was observed using a combination of Focused Ion Beam (FIB) and Atomic Force Microscopy (AFM). The AFM scans from two different modes, tapping mode, and Peak Force mode revealed that no macro-phase separation is observed for films of nanoparticles of SY-PPV/PS blended in a weight ratio of 1:5 and nano-confinement helps overcome macro-phase separation. The size and morphology results from DLS and SEM for nanoparticles for all three systems of polymers in different weight ratios reveal spherical particle formation as expected for all three polymer systems and different weight blend ratios.

Lastly, OLEDs were fabricated using the nanoparticles for MEH-PPV/PS and PFO/PS systems. The MEH-PPV/PS based nanoparticles fabricated OLEDs provided higher current efficiencies values of 2.2×10^{-4} as compared to PFO/PS based nanoparticle devices for which the current efficiencies measured were up to 3.8×10^{-5}. MEH-PPV/PS was selected as the system for further device fabrication due to the nanoparticle blend providing better efficiencies, low leakage current and reproducible and stable OLED devices.

Contents

1- Introduction

Quantum Mechanics has opened gateways to the field of 'Molecular Electronics' which has grown in importance over the course of last two decades. Within the field of Molecular electronics, Organics Light Emitting Diodes (OLEDs) have established themselves as a popular device with functions and applications in mobile phone screens, lighting displays and large-scale panel lightings. The first breakthrough in polymer electronics was realized in 1977 when the first conducting polymer, the chemically doped poly-acetylene was reported [1]. In the last decade, polymers-based OLEDs or PLEDs have garnered interest due to properties of polymers such as flexibility and ease of production from solution-based methods.

There has been increased demand and interest for advancement in electronics based on improvement at the molecular scale. One such area of focus in molecular electronics has been Organic Light Emitting Diodes (OLEDs) devices [5]. The need for novel OLED devices with more functionality, flexibility has led to an interest in use of polymers as organic semi-conductors for OLED devices [6]. This has led to an increased demand for use of polymers for OLED devices due to their ease of printing, processability [7] and the cheap and easy availability of polymers. The focus has been thus on conjugated semi-conducting polymers which can conduct electricity and produce light through the process called electroluminescence. The semi-conducting polymers used in OLEDs are usually amorphous and usually have a low charge carrier mobility which means there is room for improvement to optimize the charge transport and recombination processes in these polymers-based OLEDs.

Although the semi-conducting polymers are quite useful for production of solar cells and OLEDs, there remains a great deal of room for improvement in the efficiency and the production process of OLEDs.[7, 8] There has been increased focus to make the production cheaper of Organic Photo Voltaic (OPV) and OLEDs more environmental friendly using the principles of green chemistry [9] as with every other industry due to the problems faced by the scientific community right now to tackle global warming and climate change. There has been further interest developed over the course of the last few years in production of OLEDs used for large scale processes that can be fabricated from solutions instead of vaporizing process which is primarily used in production highly efficient OLEDs for mobile phones for example [10]. Solution processing provides a cheaper alternative to the vaporizing method for production of OLEDs for lighting and other large-scale purposes. It has become desirable with considerable interest to produce OLEDs using film forming process through polymer solutions. Within this process of producing OLEDs processed from solution, lies the challenge of producing films in a solvent which is environmentally friendly and prescribes to the concepts of 'Green Chemistry' hence the film and device forming process would not have minimal carbon foot-print [9]. It has thus been the impetus to use and move towards solvents which are halogen free. Water has naturally been touted as a very attractive solvent because of ease of recycling and producing devices from water without the concern of toxicity and recyclability[9].

The mini-emulsion process as described by Landfester et. al [3, 11] has emerged as a technique to synthesize polymer-based nanoparticles in aqueous dispersions and hence avoid the need for organic solvents. Water is used as the solvent for forming nanoparticles dispersion which can then in turn be used for forming the organic emitting layer of the OLED device. This will enable to avoid using harmful and toxic halogenated solvents for OLED fabrication and reduce the cost of production and waste disposal [9]. However, there is also need to

further improve the performance of the OLEDs by improving the efficiency and by curbing the process which can result in loss of efficiency for these devices. One such area to improve the efficiency of these OLED devices is to reduce the effect of electronic traps that occur in organic semi-conductors. This has been achieved by Blom et. al [2] by the process of trap dilution of semi-conducting polymers by blending with an insulating polymer. Thus, this is an additional benefit which drives the use of nanoparticles-based polymer blends in aqueous dispersion for OLEDs. Keeping those benefits in sight, another important incentive for use of nanoparticles-based films instead of films from pure polymer blends has been the ability to use the idea of nano-confinement. There are some polymeric blends which can provide additional benefits and improved efficiencies in the OLEDs [12] when blended together however due to the general nature of the polymers itself having low miscibility with each other, these polymers when blended in bulk solutions and cast into films tend to phase separate. These phase separated regions form non-homogenous films and lead to uneven emission and lower efficiencies of the OLEDs. [13]

The idea as part of the project is to use nanoparticles to confine the polymers to a nanometer scale [12] which will allow the issue of phase separation to be addressed and will allow for fabrication of the active layer of the OLED device using blends of different polymers. This can allow the devices to be produced at lower costs, and in a greener way, while also creating an opportunity to improve efficiency and increase photo luminescence. While a lot of work has been done on nanoparticle fabrication [3] and trap dilution using polymer blends [2, 14], however the fabrication of nanoparticle based OLEDs with different blend ratios of different semi-conducting polymers has yet to be attempted. The mechanism and the state of mixing of polymers inside the nanoparticles and in the nano-confined state has also not yet been extensively investigated yet

In the first chapter, some theoretical background is presented on the working of OLEDs and the principles behind blending and dissolving polymers. In the second chapter the process of nanoparticle synthesis, the reagents used, as well as the process of device fabrication is explained. In the third chapter the results of the experiments are presented with analysis and followed by conclusion.

1.1 Semi-Conducting Polymer

A semi-conducting polymer is a polymer with an electronically conjugated backbone, i.e. consisting of alternating single and double bond in the backbone. The presence of the extended conjugated structure in the chemical structure of the polymer's repeating units means there is an extended system of delocalized pi-orbitals [17]. These de-localized pi-orbitals are able to conduct electricity through the movement of mobile electrons across the delocalized pi-orbital network [18, 19]. An electron is mobile through this extended delocalized pi-orbital system and can move along the segment of the chain length of polymer. The conduction of electric charges between different chain segments of the polymer occurs through hopping transport [17]. Intra- and inter-chain charge transport between conjugated sites can be described using the Miller-Abrahams model [20] which assumes a tunnelling mechanism. Hence, the hopping probability decays exponentially with the distance between two sites. Crystallinity and packing density affect transport rates as the chains of the polymers are more aligned and closer to each other. However, as most of the semi-conducting polymers are disordered, mobility of the electric charges is low [21]. The low mobility of the charge carriers' means fabrication of electronic devices using semi-conducting polymers have to be optimized and doped for enhance performance [22].

A semi-conducting polymer has the following electronic structure as indicated in Figure 2. The Highest Molecular Orbital (HOMO) and the Lowest Un-Occupied Molecular Orbital (LUMO) are separated by the band-gap. The HOMO and LUMO in an organic semi-conductor are analogous to the conduction band and valence band in an in-organic semiconductor respectively. As explained below, in a polymer-based OLED, electrons are injected from the cathode in the LUMO and holes are injected from the anode into the HOMO [18].

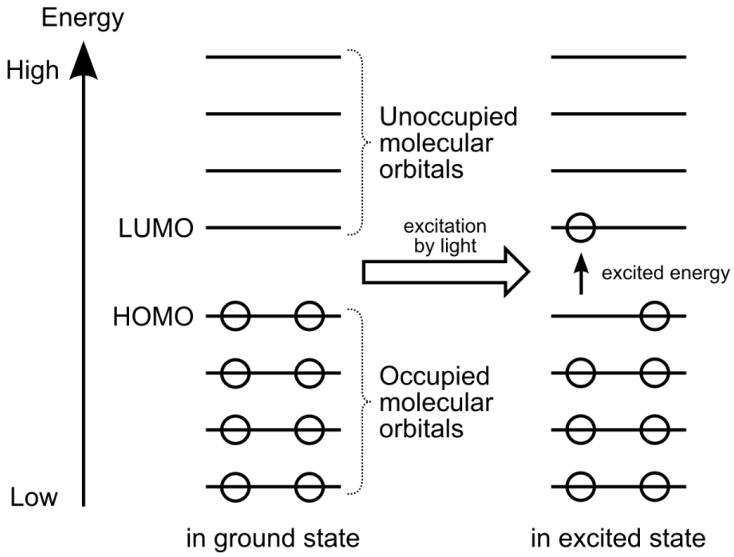

Figure 1: The electronic structure and HOMO and LUMO in a semi-conductor polymer.

.

1.2 Flory Huggins Theory and polymer miscibility

Flory-Huggins theory (FHT) provides an expression for the free energy of mixing of different polymeric or small molecular species based on a purely translational entropic contribution and a mean field enthalpic contribution stemming from mutual monomeric interaction. The theory is lattice based, whereby each monomer occupies one lattice site. The free energy (per lattice site) for a blend of two polymers is given by Eq. 1.

$$\frac{\Delta g}{kT} = \frac{\phi_A}{N_A}\ln\phi_A + \frac{\phi_B}{N_B}\ln\phi_B + \phi_A\phi_B\chi_{AB}$$

Equation 1: Flory-Huggins equation for a binary blend

, where N_A corresponds to the number of segments for polymer A and N_B for number of segments of polymer B, k is Boltzmann's constant, T is the absolute temperature and ϕ denotes volume fraction. χ_{AB} is the dimensionless FH interaction parameter which provides for an energy balance for exchanging the environment of one monomer from the pure species to the mixed state. As the value of $\ln\phi_A$ is always negative value, the

two first terms express that mixing is favourable from an entropic perspective. However, since for polymers *N* is typically large, χ_{AB} only needs to be slightly positive to make the blend immiscible.

By taking derivatives of the FH equation a phase diagram can be calculated (see Figure 2). The main features of these phase diagrams are the spinodal curve, binodal curve and the critical point. The binodal indicates the border between the single phase and coexistence region [23]. The spinodal curve represents the limit of stability. Inside the spinodal region, phase separation occurs spontaneously, whereas between spinodal and binodal demixing occurs via nucleation and growth.

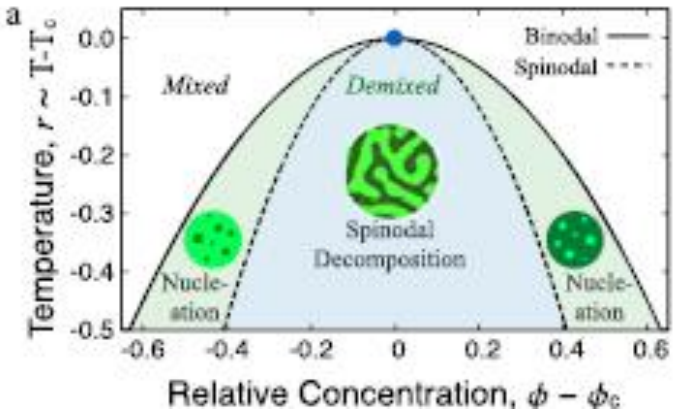

Figure 2 : Phase Diagram for Classic FHT. The Spinodal, Bi-Nodal curves are illustrated in the graph along with the phase behaviour of liquids.

The above forms one of the motivations to produce polymer blends as nano-dispersions. A geometric confinement is known to prevent phase separation.

1.3 Colloidal Suspensions, Micelles and Surfactants:

The use of surfactants is a paramount part of the process for fabrication of OLEDs using nanoparticle-based films. Surfactants are molecules which have both a hydrophobic and hydrophilic part and hence reduce surface tension when dissolved in water [24]. The molecular architecture can for instance be block-co-polymeric with parts of different affinities or salts of fatty acids. In the case of tensides, as the surfactant primarily in use in the project is a tenside, there is a hydrophilic head of Na ions and a hydrophobic alkyl tail. The surfactant in use is sodium dodecyl sulphate (SDS) **Figure 13 : Chemical structure of Sodium Dodecyl Sulphate**.

As the surfactant molecules are added to a water solution, self-assembly of these molecules starts to take place (see figure 3). This happens as when more and more surfactants molecules are added to the solution, not all the molecules can stay at the vapour liquid interface. As the concentration increases and more surfactants molecules are forced into the water solution away from the surface, they self-assemble and form micelles [24]. The hydrophilic head of the molecule protrudes outwards while the hydrophobic tail of the molecule coils inwards, remote from the water molecules [24].

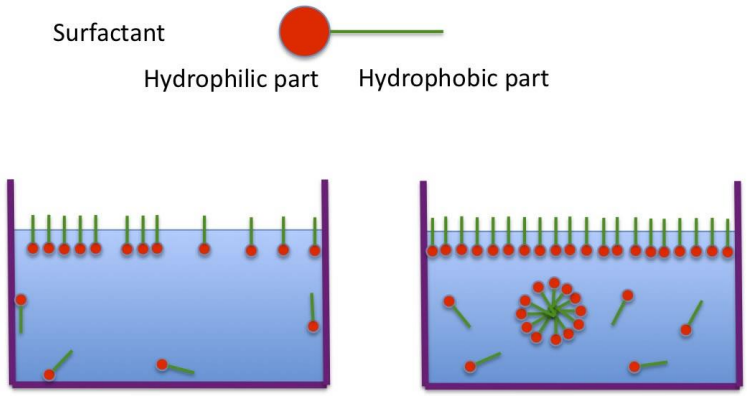

Figure 3: Illustrates the forming of micelles as CMC is reached [25]

The molecules can assemble in different structures from spherical to cylindrical micelles. The point at which the self-assembly and micelle formation takes place is called the critical micelle concentration (CMC) [24]. This can be visualized in Figure 4 which shows how the micelle formation takes place.

These micelle structures are labelled as 'soft matter' because of the ability to be deformed under the influence of shear forces [24]. The micelle structure can be broken down or the shape altered by high shear or electrostatic forces. This principle is put into effect in preparing blended nanoparticles of polymers in aqueous dispersion using mini-emulsion process. The micelles are split open by high shear forces and when assemble together back again encapsulate the polymers within them. The conjugated polymers and solvent which are also hydrophobic are more stable within the confines of the core of these surfactant micelles, rather than in the aqueous dispersion. These micelle structures with the polymer chains encapsulated in the core act as the nanoparticles of semiconducting polymers.

The colloidal dispersion of these surfactant micelles consists of dispersed colloidal particles. In order or it to be called a colloidal dispersion instead of suspension, the particles need to be stable and dispersed even after the removal of shear forces and agitation. The sedimentation of these particles is avoided if the density of these colloidal particles is similar to that of the solvent (if particles are relatively large). This is known as density matching and it stabilizes the particles against sedimentation due to gravity [24, 26]. However, the other course of destabilization force arises from inter-particular forces. These particles are attracted to each other because of Van der Waals forces [27, 28] between the particles and can aggregate [28]. In order to prevent aggregation and coagulation, and maintain the colloidal dispersion, the particles need to be stabilized. The micelle structured molecules are stabilized due to electrostatic forces [26, 29] which arise because of the presence of charged head groups on the chain of the surfactant molecules. The hydrophilic head of the surfactant is composed of sodium ions and oxygen ions. Sodium ions, when dispersed in water will ionize and its counter ion which is part of the micelle will create a negative charge across the shell of the colloidal particle and these ions being of like charges, repel each other in solution. These micelles or colloidal particles with the charged ions around the shells will act as 'macro –ions[24].' These macro ions will effectively repel each other because of electrostatic repulsion between the head groups. This stabilizes the particles from aggregation as predicted by the DLVO theory.[26]

The formation of a closed film is important for efficient charge transport and to reduce short circuits in the OLED devices. The amount of free surfactant in the aqueous dispersion will influence film formation. As

predicted by the DLVO theory [24, 30] and according to the Debye screening length [26, 29, 30], the charged particles as they interact with each other will exert a repulsive electrostatic force. An individual particle instead of experiencing individual force from its surrounding ions only experiences the mean effective electrostatic force as explained [24]. The mean force will be dependent on the amount of charged particles surrounding the colloidal particle. A higher number of charged particles surrounding the colloidal particle will lead to a cancellation of the effect of electrostatic force as experienced by the colloidal particle in what is termed as the 'screening effect'[24]. The charged particles screen the effective electric field leading to a weaker mean electrostatic force experienced by the colloidal particle. Further details of the DLVO theory and mean field theory is not described in detail in the thesis as it doesn't directly constitute part of the research questions probed in the project.

1.4 Organic Light Emitting Diodes (OLEDs)

An OLED device consists of multiple layers and produces light by the recombination process of an electron and a hole in the light emitting polymer [31]. A basic architecture for an OLED is given in Figure 4. The first layer on top of the glass substrate is a transparent anode, for which commonly indium tin oxide (ITO) is used. In this work, though, we use a thin (and hence transparent) layer of gold as anode. The anode is connected to the positive end of the electric supply and responsible for the injection of positive charges or holes in the device. On top of the anode is a layer of the polymer blend poly(3,4-ethylenedioxythiophene):poly(styrene sulfonate) (PEDOT: PSS). This layer is called the hole injection layer. The layer is coated on top of the anode to aid the transport and injection of holes into the emitting layer. PEDOT: PSS also acts as a blocking layer for electrons. The cathode, consisting of a barium-aluminium alloy, injects electrons in the LUMO of the emitting layer. The charges migrate through the emitting layer in the electric field and recombine upon encountering the same conjugated segment to form a singlet excited state, which relaxes to the ground state while emitting a photon. The wavelength of the light emitted depends on the magnitude of the bandgap of the emitting polymer. Besides this desirable emissive Langevin recombination process, competing loss mechanisms such as exciton quenching and charge trapping, typically compromise operational efficiency.

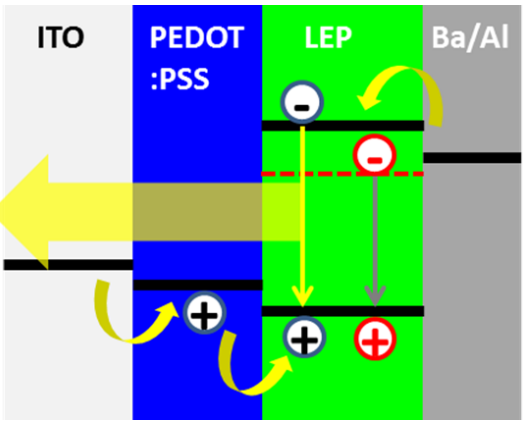

Figure 4: Schematic representation of the architecture of an OLED device. The electrons are injected at the Cathode which is of layers of Barium and Aluminium represented by Ba/Al. The electrons flow towards the anode where the holes are injected from anode to the PEDOT:PSS layer. The anode which is transparent is made up of Indium tin oxide (ITO). The step illustrated with the yellow arrow between a positive and

negative charge shows that the hole and electron will recombine in the layer of the electroluminescent or Light Emitting Polymer (LEP-green layer) to emit light.

1.5 Charge transport mechanism of semi-conducting polymer

The limitation to flow of current in a polymer can be classified as being either [32]

1. Injection limited flow
2. Bulk –limited current flow

The injection limitation in a polymer is posed by non-ohmic contacts between the polymer-metal interfaces [33]. The bulk limited flow is posed by the bulk properties of the polymer as the semi-conductor polymers being amorphous, usually have low charge carrier mobility [18, 34]. However some of the semi-conducting polymers provide close to ohmic behaviour hence the injection limitation to the flow of current is not the limiting factor anymore and it is the bulk –limited flow of charges[33]. The conduction through semiconductor polymer layers occurs and can be explained by two different current regimes, the ohmic current regime and space-charge limited current (SCLC) [35]. At low voltages, where the flow of charges is not yet bulk-limited, the polymer layer offers ohmic response to current flow. After a certain voltage is achieved, known as the threshold voltage, the transition from ohmic to SCLC takes place.[33] This transition is illustrated in Figure 5.

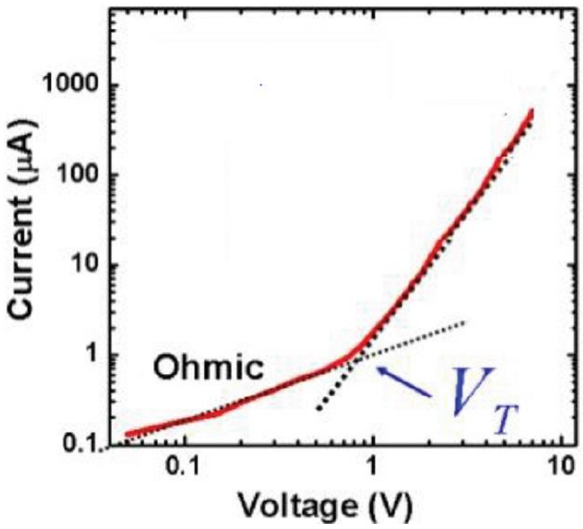

Figure 5 : ohmic and SCLC current flow in a semi-conductor polymer layer with the point where the changeover takes place called the threshold voltage illustrated as VT [33]

The space charge limited current describes the region of the current flow after the voltage is high enough for bulk injection to begin and also seemingly close when the radiative emission of light also begins. At this point the built-in field that rises due to the difference in work function between the electrodes is overcome in an OLED. [36]. However at the metal-polymer interface, the barrier height is reduced if the LUMO aligns well with the valence band of Cathode. This leads to higher probability of injection of charges from the metal to the polymer. This injection can lead to a region of space charge and space charge limited current.

If the polymer layer however is sandwiched between two metal surfaces and if one of them happens to provide ohmic contact to the polymer layer, this can remove the injection limitation to the polymer layer from the metal surface and leads to injection of charges in the polymer layer from the metal. The charges then start to get injected into the LOMO of the polymer which is now well aligned with the metal's valence band. The injection in the polymer layer continues and the charge starts to build up as the charges are injected faster then what they can flow[34].

The bulk limited flow of current in a polymer is imposed by the bulk material properties of the polymer. The mobility of the charges through the polymer layer is low so the current or charges cannot flow as fast from one electrode to the other than at the rate they are being injected from the metal layer having an ohmic contact with the polymer layer. When an external electric field is applied as in an OLED device, the charges are injected into the polymer even faster until at a point the build-up of injected charges is equal to or higher than the concentration of the intrinsic free-charges of the polymer layer [33]. The current flow is limited by this bulk limitation and combination of faster injection of charges into the polymer layer and this phenomena is called space charge limited current [19]. The current in space-charge limited current regime is now dependent on the square of the voltage rather than the voltage as in ohmic current as demonstrated by the Mott-Gurney equation for the space-charge-limited current (Equation 2) [37, 38]. Here, J presents charge current density, L the layer thickness, ε the dielectric constant and μ the carrier mobility. The SCLC is dependent is inversely proportional to the thickness of the layer represented by L and μ represents the carrier mobility.

$$J = \frac{8}{9}\varepsilon\mu\frac{V_a^2}{L^3}$$

Equation 2: Mott-Gurney model for SCLC

1.6 Electronic Trapping and SRH Non-Radiative Recombination

Besides Langevin recombination charges can also recombine though trap-assisted or Shockley-Read-Hall (SRH) recombination [39]. In this case one of the carriers, typically the electron, has been trapped in an electronic state intermediate to the HOMO and the LUMO. SRH is typically non-radiative and therefore a loss process. In fact, it results in a 'phonon' or lattice vibration instead of a photon. The trap states are energetically situated between the HOMO and LUMO of the semiconductor (see Figure 6). It has been suggested that traps in disordered organic semiconductors occur due to structural defects, as well as chemical impurities. However according an earlier study [14] the traps across different polymers were shown to be centred around 3.6 eV. The presence of these traps in different polymers at similar energy level can suggest that the traps are not mostly due to random structural defects, but rather to a generally occurring species, in this case a hydrated oxygen complex [14]

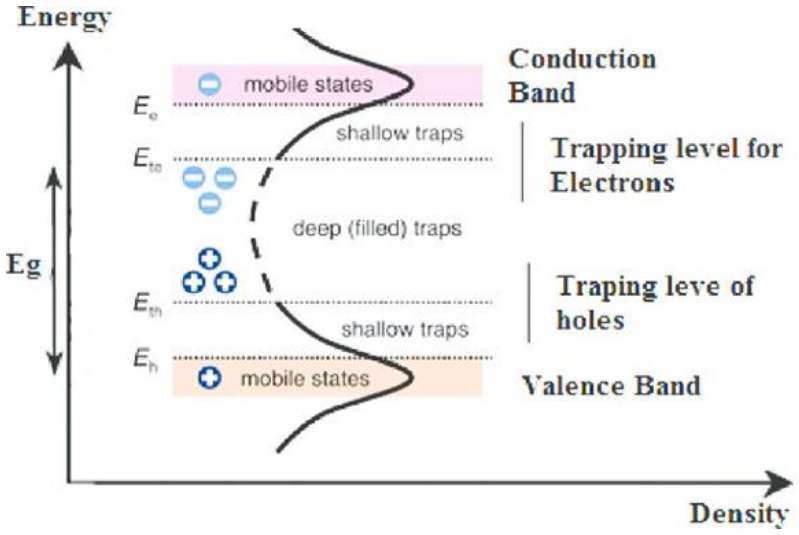

Figure 6: Conduction & Valence band & electronic traps [33]

1.7 Electron trap elimination by blending

It has been observed though by that upon blending of the semi-conducing polymer with an insulator, can lead eliminate the effect of traps. [2] This can be understood by considering the expression by Mark and Helfrich for the trap limited current density [40] (Equation 3).

$$J = N_c q \mu_e \left(\frac{\varepsilon_0 \varepsilon_r}{q N_t e^{E/kT}}\right)^r \left[\left(\frac{2r+1}{r+1}\right)^{r+1} \left(\frac{r}{r+1}\right)^r\right] \frac{V^{r+1}}{L^{2r+1}}$$

Equation 3: Trap limited current density

Here, N_c and N_t are the densities of transport and trap sites in the semiconductor; q and μ_e are the elementary charge and the electron mobility; ε_0 and ε_r are the vacuum and relative permittivity, kT is the thermal energy, V is the voltage and L the film thickness. The parameter r is given by $r = T/T_t$, with T_t the "trap temperature", which is a measure for the width of the energetic distribution of trap states. Since for disordered organic semiconductors r typically amounts to 4 to 5 [41], reducing N_c and N_t by the same factor by diluting the semiconductor with an insulator results in an increase in the current density and enhancement of the device performance, as has been shown in [13] However, as discussed above, Flory-Huggins theory tells us that polymers are difficult to mix due to the reduced translational entropy. Hence, with this work, besides aiming for a "greener" way of producing OLEDs, we also aim to show that phase separation can be suppressed by processing semiconducting: insulating polymer blends in nanoconfinement. We will use the mini-emulsion process to accomplish this and generate the nanoparticles as aqueous dispersions, from which we will cast the OLED active layers.

2 - Objectives of the Project

While nanoparticle based layers for Organic Photo-Voltaic (OPV) devices have been successfully attempted [8, 15, 16], there has not been extensive research carried out on using nanoparticle based polymer films for OLEDs due to the difficulty of film formation and high charge density in the devices. The aim of the project is to synthesize polymer nanoparticles using mini-emulsion process for different blends of semiconducting and insulator polymers. It has been reported that blending of an insulator with semi-conducting polymer can eliminate electronic traps and enhance the efficiency of bi-molecular recombination. The blended nanoparticles of an insulator and semi-conducting polymer will be used to attempt to fabricate novel OLEDs using aqueous nanoparticle-based films of different blend ratios and observe the device performance for these films. The semi-conducting polymers that are used are Super-Yellow PPV, MEH-PPV and PFO with their detailed chemical structure in section **3.2 Reagents**. The insulating polymer used is Polystyrene. Polystyrene is used because it is cheap, easy to synthesize with a low polydispersity. It should be taken into account that polymer synthesis is not an objective of the thesis and the polymer used are either synthesized in house (at MPIP) or bought from Sigma-Aldrich.

The motivation to use nanoparticle-based film instead of a pure blend film of semi-conducting and insulator polymer is due to the problem of low miscibility of polymers and their ability to phase separate. The principle of nano-confinement can in principle help overcome this problem. The mixing of polymers and the morphology of the nanoparticles is to be investigated to observe how phase mixing of the polymers is altered as within the confinement in the nanoparticle. The effect of ratio of blending on the synthesis of particles in terms of size, morphology and the device performance are to be investigated. The internal morphology of the nanoparticles is also to be investigated and the phase behaviour of the polymers within the nanoparticles. In order to better understand these systems, three different systems are used. The first is a polymer blend system of SY-PPV (semi-conductor) and PS (insulator) with chloroform as the solvent for the organic phase. SY-PPV is used because of its higher external quantum efficiency and being regarded as an efficient semi-conducting polymer. SY-PPV and PS are blended in different weight ratios in the organic phase namely 1:1, 1:3, 1:5 and 1:9. It is to be inspected that how blending the polymers in different weight ratios can alter the size of the nanoparticles and what effect it has on the OLED device performance. What is important here to note is that the other important factors which have a major impact on nanoparticle size distribution is the amount of surfactant in aqueous phase and the concentration of total polymer in organic phase which is always hence kept constant. This enables to study solely the effect of blending different semiconducting and insulating polymer in different weight ratios on size distribution and morphology of the nanoparticles. Chloroform is used as the solvent because of its favourable interactions with the conjugated bonds in the SY-PPV polymer. It is also interesting to study if altering the blending ratio will alter the shape of the nanoparticles and the blend morphology within. Once the first system is studied then the blend ratios of the polymers are applied for the second system of polymers which is of MEH-PPV and PS with toluene as the solvent for the organic phase. The third system used is PFO and PS with Chloroform as the solvent for the organic phase. Due to time constraints, not all possible blend ratios can be studied for all three systems. Instead, the blend ratios which show distinct results or are necessary to study the width of the system is used. This is a weighted blend ration of 1:1, 1:3 and 1:5 of semi-conductor : insulator polymer.

The nanoparticles for the three systems are synthesized using the mini-emulsion technique. In order to ensure the reproducibility of the recipe and the size distribution of nanoparticles, the concentration of surfactant and the total polymer concentration in the organic phase is kept constant for all three systems. As the objective is to study the size and morphology by effect of blending of a semi-conductor and insulator polymer in different weight ratio, it is important at first two keep the other two factors constant. The surfactant concentration is fixed at 150mg in 10 ml of organic phase and the total polymer concentration as 100 mg in 4 ml of organic phase.

The other objectives are concerned with analytics and analysis of the nanoparticles using different spectroscopy and analytical techniques. DLS and SEM are utilized to study the size distribution for all three systems of nanoparticles. In order to further probe the internal morphology of the nanoparticle and understand the effect of nanoconfinement on phase separation, AFM, TEM spectroscopy and DSC is applied. DLS and SEM would give information about the size and external morphology of the particle whereas AFM and TEM about the internal morphology and blending of polymers within the nanoparticle.

3- Experimental

3.1 Devices and Methods

3.1.1 Transmission Electron Microscopy (TEM)

TEM microscopy uses a light beam of electrons to penetrate the sample. The sample is prepared in the form of a thin film and irradiated with beam of electrons. A series of electromagnetic lens enable to focus the electronic beam. When this electron beam passes through the thin layer of the sample, some electrons are scattered, and some penetrate through the sample. The transmitted electrons strike a screen and the lenses are used to focus the beam to create an image. TEM has been used to study the morphology within the nanoparticle samples. The idea is to study the outermost shape of the particles to observe how the blending can affect the shape of the particles and to observe any phase separation within the nanoparticle as well to see if the polymers phase separate under nano confinement or remain miscible. The presence of contrast difference can indicate phase separation within the particle. The contrast in images arises due to variation of the electron scattering depending on the local structures and composition of the specimen, i.e. atomic number, thickness and density.[42] Figure 6 illustrates the working principle of a TEM microscope.

Supplier: JEOL; Model: JEM-1400
Device parameters: Acceleration voltage: 120kV; Cathode: LaB_6 (thermionic emitter)

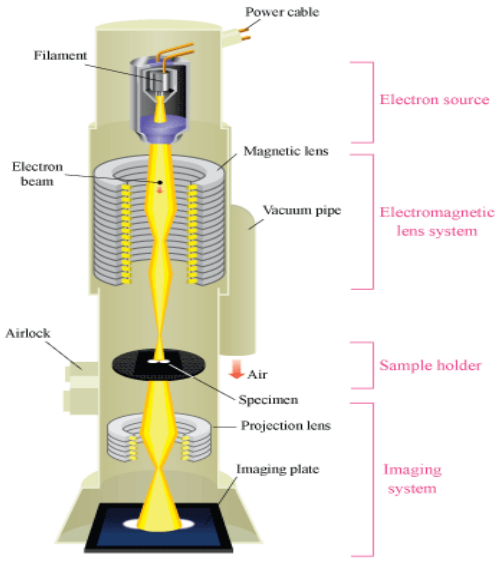

Figure 6: Working Illustration of TEM

3.1.2 Scanning Electronic Microscopy (SEM)

SEM microscopy uses a light beam of electrons to bombard the surface of the sample. The electrons which are reflected or deflected by the particles are detected by the detector and analyzed to create the image [43]. The SEM is able to make scans of the surface and has been used to study the morphology and presence of the nanoparticles. The SEM sample for this project is prepared using drop casting solution on a silicon substrate.

The SEM was also used to analyze the surface morphology of the films of the nanoparticles to study the film formation of nanoparticle layers on OLEDs. Figure 7 gives the schematic for working of SEM.

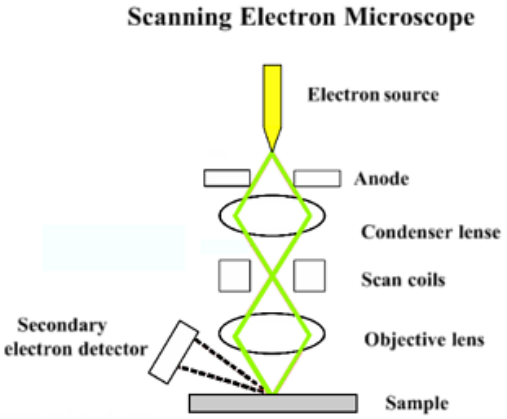

Figure 7: A typical depiction of working of SEM

Equipment used: LEO Gemini 1530 Scanning Electron Microscope
Specified point resolution: 1.0 nm (@ 30 kV and WD = 4 mm)

3.1.3 Atomic Force Microscopy (AFM)

AFM, known as atomic force microscopy, has been incorporated to study the morphology of the different films of polymeric nanoparticles formed while making devices. The technique has also been put to use in addition with the Focused Ion Beam (FIB) spectroscopy to probe and observe the morphology and intermixing of the polymers within the particle. AFM can be used to probe the morphology and conduct scan of the surface of films and solids in a non-destructive way. [44] AFM works by using a laser beam which is focused on the back of a cantilever tip which scans the morphology of the surface of the sample. As the tip moves on the surface, the deflection of the laser beam is picked up by a detector and the signal is used to create an image of the surface morphology. This principle is used to study the morphology of the nanoparticles formed and also more specifically to probe the center of the nanoparticles. FIB is used to polish away or cut through a layer of nanoparticle film using a focused laser beam which etches away the layer by sputtering ions [45]. This polished surface is then probed by the AFM cantilever which scans through the morphology of the surface to analyze the state of polymers within the nanoparticle.

Equipment Used: Dimension Icon with ScanAsyst
Supplier: Brucker

3.1.4 Thermo-Gravimetric Analysis (TGA)/ Dynamic Scanning Calorimetry (DSC)

TGA and DSC have been performed to study the effect of change in the glass transition temperature for nanoparticles of different ratio of polymer blends. TGA has been used to record the temperature at which the polymer decomposes so that when DSC is performed, the polymer samples are heated below the decomposition temperature. The decomposition temperature of the polymer was analyzed by the mass decay

curves of TGA. DSC was then used to study the effect of blending of different ratios and how the T_g or glass transition is altered by the blending and which polymer has a bigger impact on the blending on the glass transition temperature of the nanoparticles. This was also important for the annealing process of the polymer films as blends with a different glass transition temperature will need to be annealed at different temperatures and for different durations.

TGA Equipment - Supplier: Mettler Toledo, Model: TGA-851
DSC Equipment - Supplier: Mettler Toledo, Model: V3.10

3.1.5 Dynamic Light Scattering Spectroscopy (DLS)

DLS uses a laser beam at a certain angle to scatter light for the analysis of the size distribution in a dispersion of nanoparticles. The scattering of the light beam at different angles is collected by the scanner and analyzed. The DLS device uses a co-relation function to extract data about the size and population of particles from the light scattering measurements. The Z-average is calculated using the software applied polynomial fit to the co-relation function. The constant of the polynomial gives the value for the Z-Average which is the average value of the diameter of the particles assuming a Gaussian distribution and a single species population. The DLS provides the Z-average and the poly-dispersity index (PDI) or the spread of the distribution. This is not o be confused with the PDI used for polymer synthesis as the value of PDI generated from the DLS software program describes using the polynomial function the width of the peak of the population of nanoparticles. The DLS has been used to study the formation of nanoparticles and their size distribution corresponding to change in blend ratios for different polymers as well as to study the effect on particle size distributions of the surfactant concentration. Measurement of particle size distribution was done using the DLS equipment by Malvern at 25^oC.

3.1.6 X-Ray Photoelectron Spectroscopy (XPS)

XPS is used to irradiate the sample with high energy X-ray beams. It is a method to probe the surface of a sample up-to molecular scale to determine the surface composition of a sample.[46] The sample can be probed up to a depth of 10 nm. When the high energy X-rays incident the surface of the sample, the electrons in specific bound states are excited and break away from their bound configuration. The specific energy, also called as binding energy, required to break an electron away from its nuclear attraction is unique to each element and can thus be used to identify the element present in the surface. It also influenced by the chemical environment of the sample which can cause certain shifts in the bind energy values. The idea is to use XPS to probe the nanoparticle samples in depth and to understand the morphology within the particle.

Equipment- Kratos Axis Ultra DLD

3.1.7 Surface Tension Measurement

The surface tension equipment has bene used to measure the surface tension of the aqueous dispersion after the dialysis of the nano-particle based dispersion to remove the surfactant. The surface tension measurement

helps maintain the reproducibility of the devices. The films are formed from nanoparticle dispersions which are dialyzed and it is paramount to maintain the amount of surfactant in the dispersion to ensure an even and closed film and to prevent excessive agglomeration. These values have been previously calculated by the group through trial and error as for these range of values, closed films of nanoparticles are achieved at the lowest possible surfactant concentration.

Equipment used – Supplier: Data Physics, Model: DCAT 21

3.1.8 Thermal Scan

The thermal scan equipment is used for checking and measuring the performance of the devices after the fabrication of the device is complete. A sweep of voltage is applied across the electrodes on the OLED device and the resulting current flow and the photo-current flow and light output is measured. A photodiode measures the light output from the OLED device. The scans are made for different areas of the device and at different voltages to see observe the current-voltage characteristics. The results are analyzed and stored by the 'OLED' software custom made for the institute. These scans are plotted to measure the current density at different voltages, the leakage current in the devices and to measure the arbitrary efficiency of the devices using the fact of how much photo-current is generated from the electric current. The thermal scan equipment can also be used to measure the dependency of current with temperature, however the thermal scans itself are measured only for electron only devices as the electron current is strongly temperature dependent and gives valuable information when measuring electron only devices [17].

3.2 Reagents

The polymers used were PEDOT: PSS, Polystyrene (PS), Poly[2-methoxy-5-(2'-ethylhexyloxy)-1,4-phenylene vinylene] (MEH-PPV), Super-Yellow PPV and Polydioctylfluorene (PFO). PS (M_w : 80,000 g/mol), PFO (M_w :700,000 g/mol) and MEH-PPV M_w (250,000 g/mol) were used as synthesized within the MPIP institute.. Figure 8, 9, 10, 11, 12, and 13 indicate the chemical structures of these polymers respectively. Super-Yellow PPV (Mw 1.5 million g/mol) was bought and used as it is from Sigma-Aldrich.

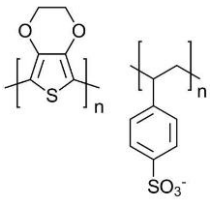

Figure 8 : Chemical Structure of PEDOT: PSS

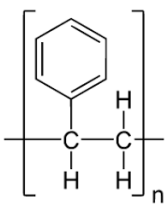

Figure 9 : Chemical Structure of Polystyrene

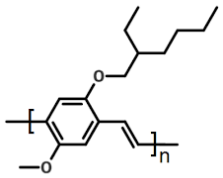

Figure 10 : Chemical structure of MEH-PPV

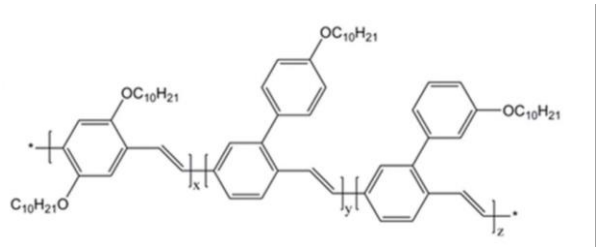

Figure 11 : Chemical structure of Super-Yellow PPV

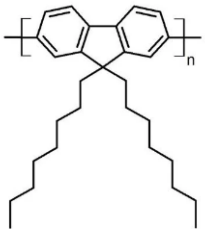

Figure 12 : PFO chemical structure

The organic solvents used were Chloroform, Toluene (anhydrous, 99.8%). Surfactant used was Sodium Dodecyl Sulphate (SDS). The chemical structure is indicated in Fig. 15

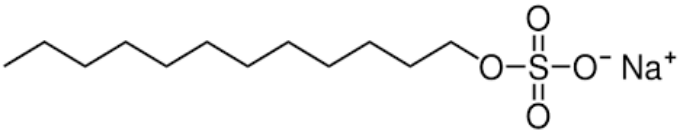

Figure 13 : Chemical structure of Sodium Dodecyl Sulphate

3.3 Synthesis of nanoparticles

3.3.1 Mini-Emulsion Method

The nanoparticles are prepared using mini-emulsion method. The method uses an aqueous dispersion of surfactants and ultra-sonication process to prepare nanoparticles [3].

The polymers, both the insulator and the semi-conductor, are first dissolved in an organic solvent such as Toluene or Chloroform. The organic mixture is then added to the water and surfactant mixture. Sodium Dodecyl Sulphate (SDS) is used as the surfactant for the mixture. The surfactant is added as a stabilizer to stabilize the polymeric nanoparticles in hydrophilic water solution after they are formed [11]. The organic mixture is added to the aqueous dispersion and the dispersion is stirred at 1250 rpm at room temperature for 1 hour.

After the stirring, the mixture, is subjected to agitation using high revolutions with the UV-tip sonicator. This helps to disperse the polymers through-out the mixture due to high shear forces acting on the mixture. The total sonication time or the mixture is 6 minutes. The mixture is subjected to revolutions of 70% amplitude for 30 secs and a pause for 10 secs for a total duration of 6 minutes. The polymers, which are hydrophobic, upon contact with water, are forced to assemble into the core of the surfactant micelles along with the organic solvent phase, hence forming nano-emulsions as now it is the organic liquid phase dispersed in the liquid aqueous phase hence an emulsion. It is favourable for the organic phase to stay within the enclosed surfactants micelles with the hydrophilic part of SDS stabilizing the micelle in the water solution. The organic solvent is put to evaporate as soon as the sonication process is over and the continuous escaping of the organic solvent and with it the organic phase, ensures the polymers stay within the confines of the surfactant micelles where they are protected from the hydrophilic environment. As the organic solvent evaporates, a nano-dispersion is achieved of nanoparticles, which are solids, dispersed in a liquid phase. What this also achieves is that now both polymers are supposedly blended within the particle or even if they do phase separate can do so within the domain of this nanoparticle. They are now as to be termed, under ´nano-confinement´ and cannot escape the micelle structure of SDS. The mixture after the UV- sonication is left to stir over night in order to allow for the organic solvent to evaporate. Fig. 14 and Fig. 15 show the schematic of mini emulsion process step-wise. The presence of surfactant helps to stabilize these particles in water as the organic solvent is evaporated. The evaporation process was tuned as per the organic solvent and their relevant boiling points. The excess surfactant which is present after the removal of the organic solvent is then removed from the solution by dialyzing the nanoparticles dispersion [47].

After the UV-sonication, the nanoparticles/aqueous dispersion was left to stir at 80^{o}C for 8 hours and then at 70^{o}C over night for the Toluene to evaporate as the boiling point of Toluene is 110.6^{o}C. The flask was covered with aluminium foil with small holes so as to allow toluene to evaporate. As Chloroform was used for Super-Yellow PPV and PFO, the dispersion was left to stand over night at room temperature for chloroform to evaporate.

Equipment used - Branson Digital Sonifier, Model: W-450D

Amplitude	**70%**
Run-Time	**6 minutes**
Program	**30 secs run time, 10 secs pause**
Evaporation temperature for organic phase	**Toluene 80^{o}C (36-42 hours) , Chloroform 25^{o}C over-night**
Total amount of Polymer used	**100 mg**
Total amount of Surfactant Used	**150 mg**
Total amount of Organic Solvent used	**4 ml**
Total amount of de-ionized water used	**10 ml**

Table 1: conditions and parameters used during mini-emulsion process

Below is the schematic for the mini-emulsion method for the preparation of nanoparticles.

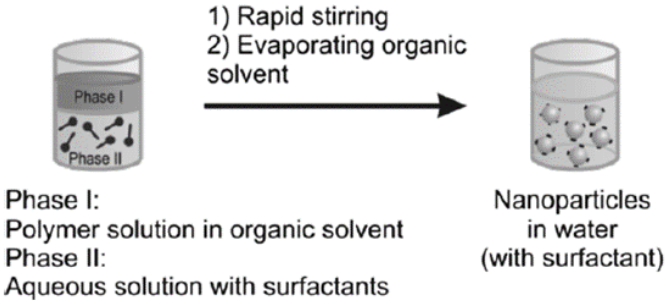

Figure 14: Schematic of Mini-Emulsion Process

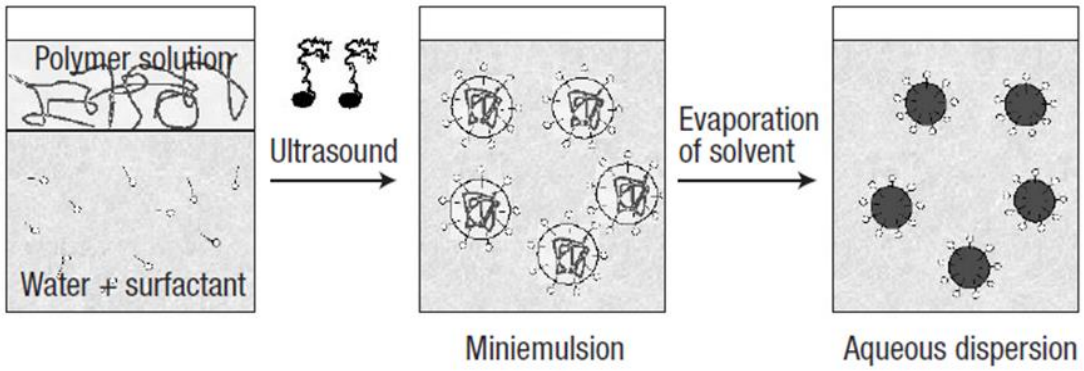

Figure 15: Another schematic of Mini-Emulsion Process

As the time required to evaporate the organic solvent which is Toluene for MEH-PpV/PS nanoparticles was considerably high, other techniques were explored for faster and efficient removal of the organic phase after the sonication process. One such technique which was explored was the use of rotary evaporator to evaporate the organic solvent. This could reduce the time for the synthesis of the particles. However another benefit what it could possibly provide as reported [48] was improved blending of polymers within the nanoparticles. The problem with using the technique was the presence of SDS which causes foaming and spitting of the solution as the pressure is lowered to boil out the organic solvent. This technique hence wasn't applicable to the system and the previous method of evaporating the solvent through heating was sustained and reproducible polymer nanoparticle batches produced.

3.3.2 Choice of Organic Solvent

Chloroform was used for Super-Yellow PPV/PS nanoparticles as well as PFO/PS nanoparticles, whereas Toluene was used for MEH-PPV/PS particles. The choice of organic solvent was also important. The solvent was required to be immiscible with water for the nanoparticle formation to work. However, the boiling point was required to be neither to low or nor too high. A low boiling point solvent for example di-chloro methane cannot withstand the mini-emulsion process [49] and would evaporate during the UV sonication where lots of heat is generated. The other important aspect of choice of solvent is their interaction with the semiconductor polymer itself and its effect on film formation. [16]

Toluene was chosen as the organic solvent for MEH-PPV due to the aromatic backbone of MEH-PPV and then long aliphatic side chains.[9] Aromatic solvents such as Toluene or di-chlorobenzene have a favourable interaction with the aromatic backbone [50] which will allow the polymer to unfurl in the solution and will allow the aromatic rings to be closer to each other thus enhancing the π-π interactions between the aromatic segments of solvent and polymer [51]. This straighter and open chain will allow for better hopping transport and conduction through the delocalized π-π bond in MEH-PPV and will lead to longer conjugation lengths and percolation. [50] The non-aromatic solvents such as chloroform can prevent that as they have more favourable interaction with the aliphatic side chains and thus causes the polymer to coil up. The solvent wants to maximize interaction with the aliphatic side chains and minimize interaction with the aromatic backbone. This causes the aliphatic side chains to be present in between the aromatic backbone, creating torsional defects and hence reducing the length of conjugation segments. Chloroform was used for synthesis of Super-Yellow PPV/PS particles. Super-Yellow has a triple block co-polymer structure and an extensive aromatic system as well as

aliphatic side chains, however the presence of the extensive aromatic network ensures that the conjugation length is significant for effective delocalized π-π bond interactions over the network and an effective hopping transport takes place.

3.3.3 Dialysis of the Aqueous Dispersion

The particles are prepared using the mini-emulsion method which has now produced an aqueous dispersion with nanoparticles and surfactant. The excess surfactant particles have to be removed as it interferes with the device performance. The aqueous dispersion of the nanoparticles is now dialyzed in de-ionized water for a period of 15-16 hours. The duration was analysed using the calibration curve as indicated in Fig. 16, by measuring the surface tension of the samples at different time scales.

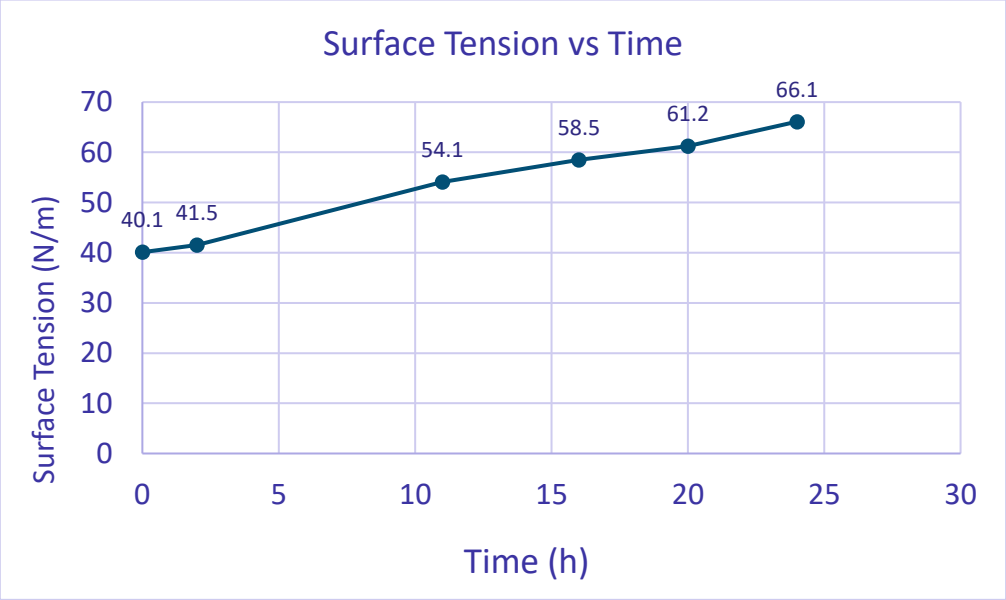

Figure 16: Surface Tension measurement for SDS with time

The tubing used for dialysis was made of re-generated cellulose bought from SERVA. The dialysis tubing had a diameter for 21 mm. The tubes were first cleaned with distilled water and washed in de-ionized water bath for 1 hour to remove an excess loosely bound cellulose.

2.3.4 Centrifuging

The centrifuging process is performed for the nanoparticle batches after the dialysis. The batches are concentrated to 33.3 mg/ml concentration which ensures that the particles are concentrated enough to coalesce into a closed film during the film and device fabrication process. The centrifuging process is performed in Sigma centrifuge 3-30 KS using centrifugal filter tubes bought and used as it is from Merck GmBH.

These tubes have a filter present which allows the water molecules to pass through but retains the nanoparticles. The size of the mesh is 100,000 NMWL.

The samples are loaded into centrifuging tubes and run at 8000 rpm for 6 minutes. The excess water is removed through the filter and the concentrated aqueous nanoparticle dispersion is now extracted and passed through another filter of 0.45 microns to remove any large aggregates which would hamper the formation of a uniform and closed film.

3.4 Fabrication of OLEDs

The fabrication of the OLEDs was partially done in the clean room in order to avoid any dust particles from interfering with the film formation in the device. The fabrication of the devices starts with first the cleaning of the glass substrates.

The glass substrates are each cleaned for three minutes with neutral soap solution to remove any dust or other impurities which can affect the film formation of the nanoparticle layers. The substrates are then in order immersed in bath of distilled water, acetone and ethanol for further purification and then dried using nitrogen gas. The glass substrates are placed in the oven and dried at 140 ^{o}C for ten minutes to ensure that the substrates are dry. Glass is chosen as the material to prepare devices on as it is transparent and would allow light emitted from the device to pass through.

After the cleaning process, the glass substrates are evaporated with layers of Chromium and Gold which will act as the Anode. Gold (Au) functions as the primary layer and acts as the Anode. The layers of chromium and gold are 1 nm and 20 nm thick respectively. Chromium is primarily used as Gold doesn't adhere well to the glass substrates, hence, to make the layer of Gold stick to the substrate an initial layer of Chromium metal is evaporated.

After the evaporation of the Gold layer, a layer of PEDOT: PSS (Clevios 4083) is coated on the devices. This layer acts as the hole injection layer as it facilitates the injection of holes into the OLED device from the Gold anode. The film of PEDOT:PSS is coated using spin-coating process. The substrates are spin coated first at a speed of 1200 rpm for 60 secs to spread to ensure smooth and even spreading of the polymer solution on the glass substrate and then at a speed of 4000 rpm for 20 secs to induce drying of the layer. However, before the coating of the layer of PEDOT: PSS on the substrates, they are first subjected to UV-ozone treatment in the oven, whereby making the glass substrates a better surface for the PEDOT: PSS layer to wet and spread evenly. Indium Tin-Oxide (ITO) is the standard anode used or OLEDs with pure polymer blends. However, it was observed that the wetting and spread of nanoparticle films was not homogenous with the presence of ITO as the anode. The exact reason for this behaviour is not known as of yet. One possible explanation could be the rough edges on the microstructure of ITO disrupts the formation of a closed layer of nanoparticles. Hence, Gold has been used as the anode for OLED fabrication with nanoparticles-based films. After the substrates are coated with PEDOT: PSS layer, they are left to anneal for one hour at 200^{o}C for the layer to dry and so that it is not washed away when the next layer of polymer nanoparticles is further coated on top.

After the coating and drying of the PEDOT: PSS layer, the layers of nanoparticle are coated on top. These layers that are formed of the nanoparticles of semi-conducing polymers, either the PPVs or PFOs and are responsible for the light emission in an OLED. Before coating of the nanoparticle layers, the substrates are subjected to electronic plasma treatment for 5 secs at a power of 100 watts. The plasma treatment improves conductivity and wettability of the dried layer of polymers by charging the surface so the next layer of aqueous nanoparticles adheres well and can thus form a closed film. The layers of nanoparticles are coated using a spin coater. The spin coater is run for 30 secs at 1000 rpm to spread the layer of the polymer evenly and then at 4000 rpm for 30 secs to enable drying and closed film formation. After the coating of the first layer of the nanoparticle film, the substrate is left to dry on a hot plate for five minutes at 70 ^{o}C. The process is repeated with the substrate as it is treated with plasma again before the next layer is spin coated on top. This procedure was repeated thrice initially to form closed film structure of polymeric nanoparticles. However, upon further experimental analysis and trials, the procedure was repeated with one spin coated layer and two spin coated layers of nanoparticle films instead of three layers. The two coated spin layers were able to provide closed film formation and better performance and lower thickness for the films. The thickness of the films is also instrumental in the performance of the OLED devices [17]. According to Equation 4, increased thickness will have lower space charged limited current density for the same voltage applied. Hence, as two layers of spin-coated nanoparticles are able to provide closed film formation and reduced thickness, the impetus is now to fabricate devices with two spin-coated layers instead of three.

After the final layer is formed, the almost to be ready devices are now kept for annealing at a set temperature for two hours in a nitrogen-based environment. The set temperature varies with the choice of polymers used. The films were annealed at 110^{o}C for MEH-PPV/PS based nanoparticles, at 140^{o}C for Super-Yellow PPV/PS and at 120^{o}C for PFO/PS based films. The annealing process helps the particles to coalesce together to form an even and closed film which is important to prevent short circuit in the device and for enhanced performance [52].

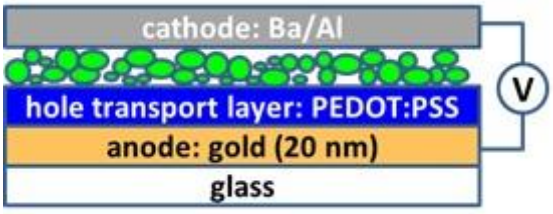

Figure 17: OLED device structure fabricated using nanoparticle based films for this system. The layers are as explained in the text.

After the annealing process, the final step is to evaporate the cathode on top of the device. For the cathode, two layers are used, one of Barium and then on top is the layer of Aluminium. Barium has a higher work function then Aluminium and can provide an intermediate step to facilitate swift injection of electrons from the cathode into the semi-conducting polymer layer. The layer of Barium is 5 nm thick and is then followed by a 100 nm thick layer of Aluminium. Fig 17 and 18 illustrate how the layers stack up to make the OLED device based on nanoparticle-based light-emitting active layer. The fabricated OLEDs are then analysed using current-voltage frequency sweeps and a photo-current detector to determine the current voltage characteristic graphs and measure the light output from the devices.

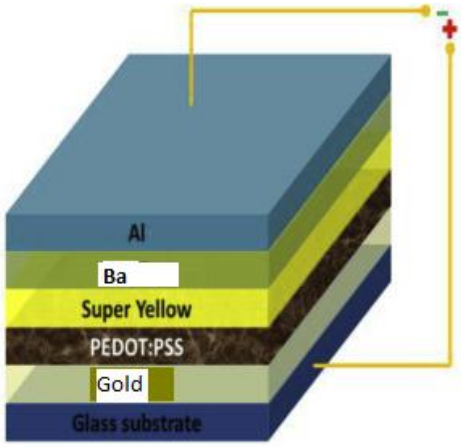

Figure 18: The structure of the OLED device which was fabricated using SY-PPV as LEP

4 - Results and Discussion

4.1 DLS (Dynamic Light Scattering spectroscopy)

The DLS was used to measure the size, creation and presence of nanoparticles in the solution. The nanoparticles were fabricated using the mini-emulsion method as explained in the section 3.3.1 Mini-Emulsion Method. The nanoparticles were synthesized for different semiconducting polymer and insulating polymer blended in different weight ratios. As indicated in Table 2: Nanoparticle batches of Super-Yellow PPV and Polystyrene, 3 and 4, the two polymers were blended in different weight ratios (mg) and the blend ratios was adjusted whereas the total amount of polymer for the organic phase as in the recipe was always kept constant to 100 mg as indicated in Table 1: conditions and parameters used during mini-emulsion process .So for example a SY-PPV 1:3 PS blended nanoparticle dispersion is synthesized from 25 mg SY-PPV and 75 mg PS.

Polymer Sample	Size (nm)	Pdi
SY-PPV 1:1 PS	76.1	0.204
SY-PPV 1:3 PS	70.5	0.148
SY-PPV 1:5 PS	66.5	0.163
SY-PPV 1:9 PS	59.5	0.156

Table 2: Nanoparticle batches of Super-Yellow PPV and Polystyrene

Batch	Size (nm)	Pdi
MEH-PPV 1:1 PS	57.7	0.283
MEH-PPV 1:1 PS (s)	46.8	0.265
MEH-PPV 1:1 PS (Chl)	70.5	0.247
MEH-PPV 1:3 PS	59.6	0.256
MEH-PPV 1:5 PS	62.5	0.229

Table 3: Nanoparticle batches of MEH- PPV and Polystyrene

Batch	Size (nm)	Pdi
PFO 1:1 PS	54.9	0.262
PFO 1:3 PS	61.1	0.266

Table 4: Nanoparticle batches of PFO and Polystyrene

The aqueous dispersion of the nanoparticles batches as indicated in Table 2, 3 and 4 is loaded into the disposable plastic cuvettes and then inserted into the machine for analysis. Fig. 19 shows results for different batches with DLS. A single homogenous peak in the spectrum indicates a single, homogenous population of nanoparticles for the consequent polymer system with no impurities and a successful synthesis. The colour coding for the different polymers follows their light emission spectrum, with blue for PFO, Red indicating mEH-

PPV and Yellow for SY-PPV. The mean value of the bell curve as obtained from the software indicates the average size of the population of the particles. Table, 2, 3 and 4 contain the average size of the different batches of polymers blended at different ratios. For the SY-PPV:PS blended nanoparticles, the trend clearly indicates that increasing the amount of polystyrene by weight ratio decreases the size of the particles because of the much smaller molecular weight of polystyrene compared to Super-Yellow PPV. As SY-PPV is reduced in weight ratio, from a 1:1 blended nanoparticle to a 1:9 blended nanoparticle, the size decreases. A similar trend was not observed with MEH-PPV possibly because of much lower molecular weight of the polymer.

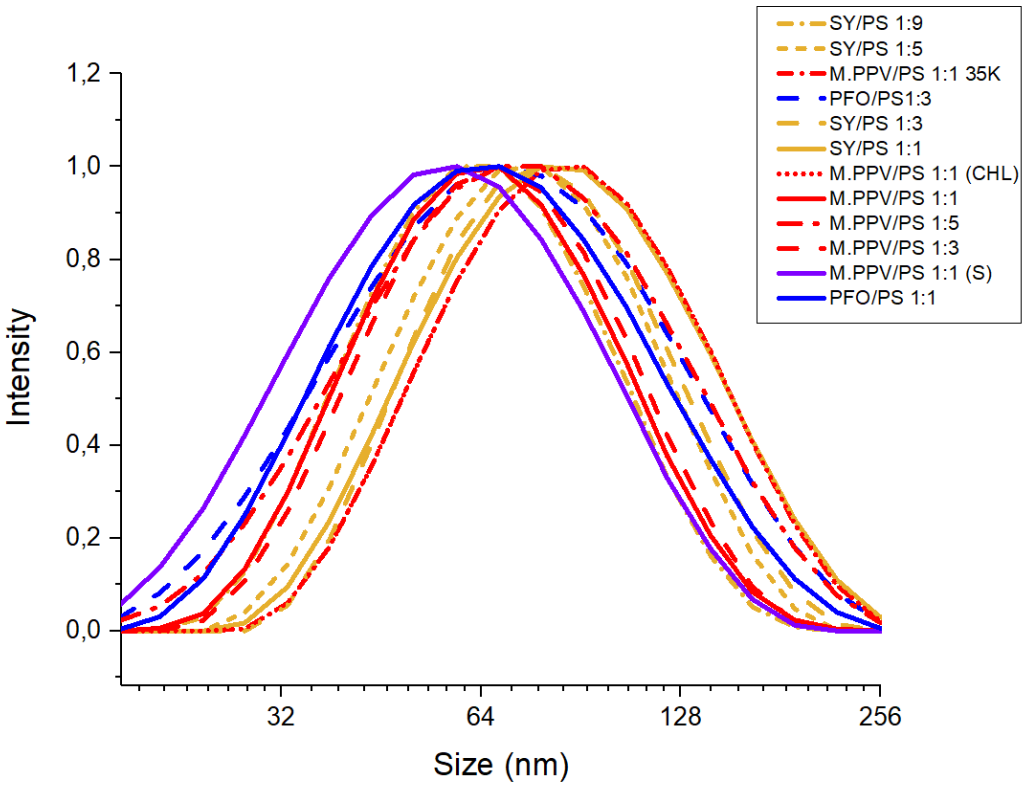

Figure 19: nanoparticle size distribution with DLS

The batch titled 'MEH-PPV 1:1 PS (s)' was the batch with the smallest average population size of nanoparticles that were synthesized. It has been observed that during the ultra-sonication process, placing the glass vial as such that the tip of the UV sonicator is as close to the bottom of the glass vial as possible and right in the center leads to particles formed with lower average size and the subsequent batches synthesized also had similar average size of the population of the nanoparticles. This could stem from an even agitation process and even distribution of the shear forces hence a more homogenous population. It is important to perfect the synthesis technique with practice as if the tip is in too close proximity to the bottom of the vial, it can lead to the rupture of the glass vial.

It can be concluded using DLS that the mini-emulsion method has worked effectively for synthesizing nanoparticles of different polymer-based systems. The nanoparticle dispersion was stable for all the different semi-conducting and insulating polymer blended dispersions which is displayed by a single measurement peak

for all samples respectively. This also highlights the reproducibility and robustness of the recipe that several different blends of polymeric nanoparticle dispersions can be synthesized using this technique.

4.2 Scanning Electron Microscopy (SEM) analysis

SEM scans were performed of both the nanoparticle dispersions and the films formed. SEM analysis was required to prove and confirm the existence of nanoparticles and to study their morphology for different blends of polymers and in different ratios. The samples were prepared by drop casting nanoparticle aqueous dispersion on silicon substrates and allowing it to dry and a film being formed. The aqueous dispersion was diluted with de-ionized water with ratio of 1:3. The scans were carried out using SEM at the institute without gold sputtering to avoid destroying and interfering with the structure of the nanoparticles. The particles appear to be spherical in shape which was expected to be as per the spherical shape of the SDS micelles which forms the shell of the nanoparticles. There are some deviations observed in the shape of the nanoparticles in SEM scans for SY/PS as observed in Figure 25 where some particles appear to deviate from the spherical shape which is synonymous with particles formed using mini-emulsion process. This could be due to the high molecular weight of SY and the mixing with polystyrene being not a straightforward process during the evaporation of the organic phase (chloroform). The deviation in surrounding temperature and rate of evaporation can hence induce slightly different morphological structure of the nanoparticles. However, SEM analysis provides no further details of the structure within the nanoparticles to be observed. Fig 20 and 21 demonstrate formation of film of particles observed in SEM scans of films of nanoparticle blends of SY: PS and MEH-PPV: PS of similar magnifications. The SY: PS particle appear more prominent in the film because of larger size compared to MEH-PPV: PS nanoparticles.

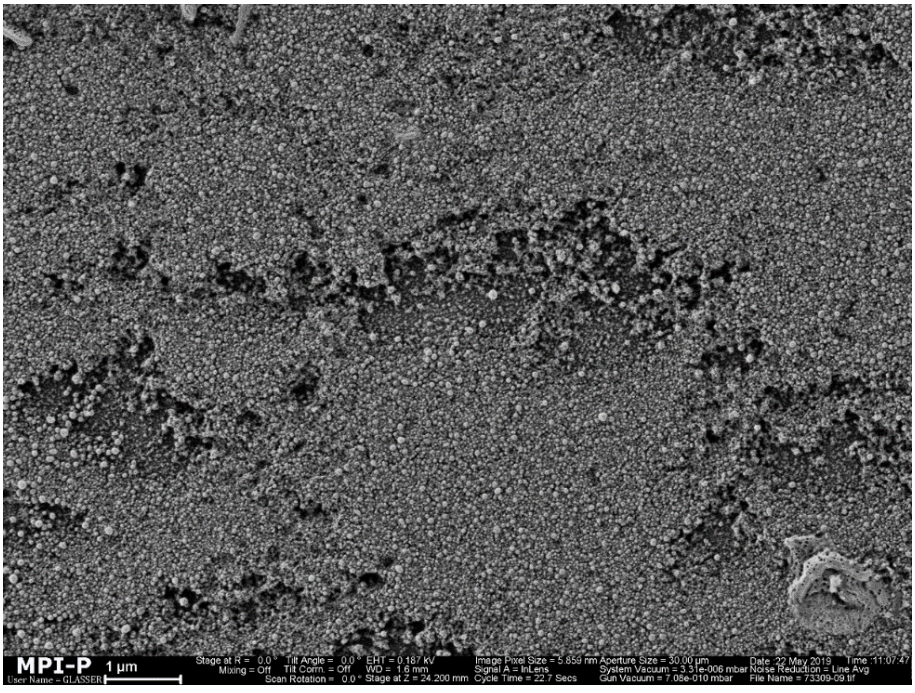

Figure 20: SEM scans of the SY-PPV/PS 1:1 nanoparticles

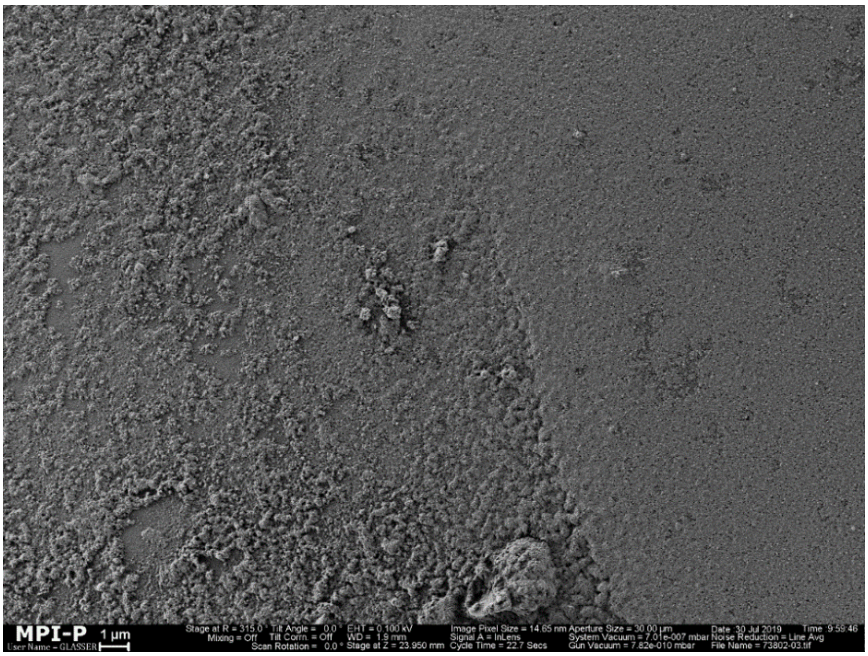

Figure 21: SEM scans of the MEH-PPV/PS 1:1 nanoparticles

Upon further magnification as indicated in Fig. 22 and 23, it can be clearly observed the presence of nanoparticles in the aqueous dispersion. The particles appear to have similar spherical morphology for even two different polymer blend system.

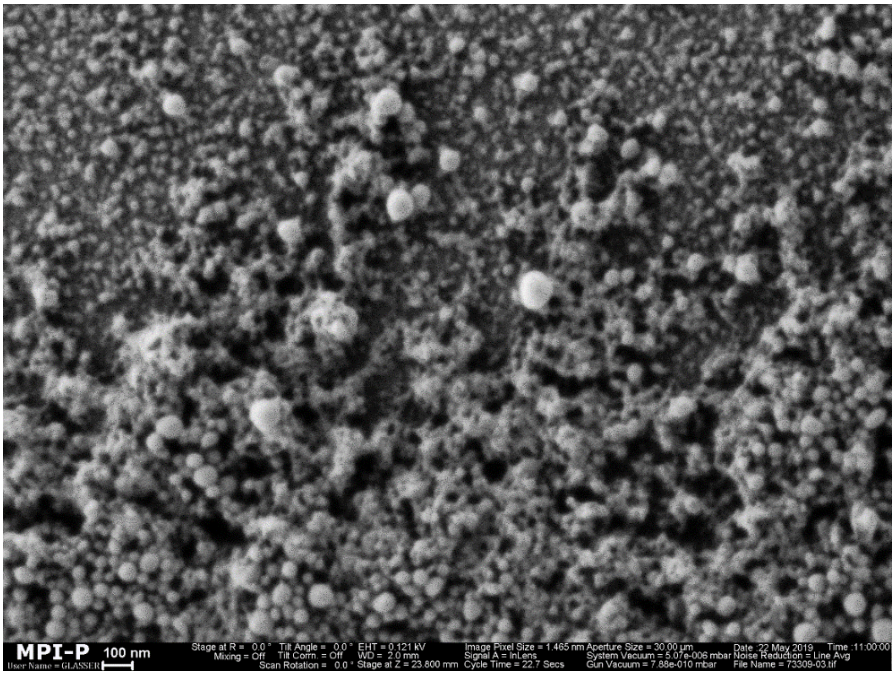

Figure 22: SEM scans of the SY-PPV/PS 1:1 nanoparticles

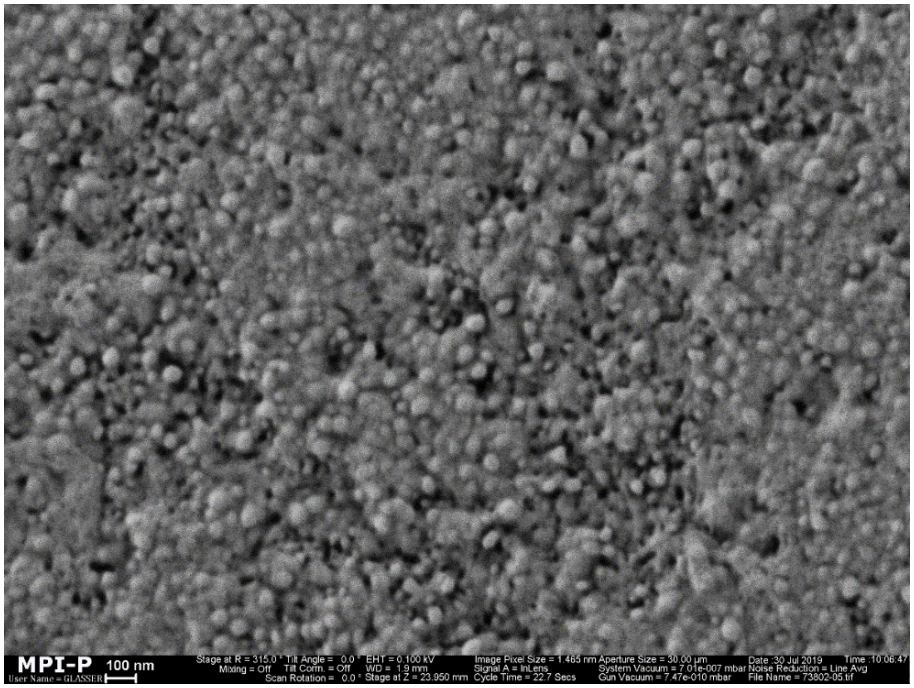

Figure 23: SEM scan of MEH-PPV/PS 1:1 nanoparticles

Further magnification was attempted to observe the actual size of the particles in order to confirm the data obtained by DLS measurements. It can be observed in Fig 24 and 25 that SY:PS nanoparticles are on average larger in size and correspond to the average size of 70 nm as obtained from DLS measurements.

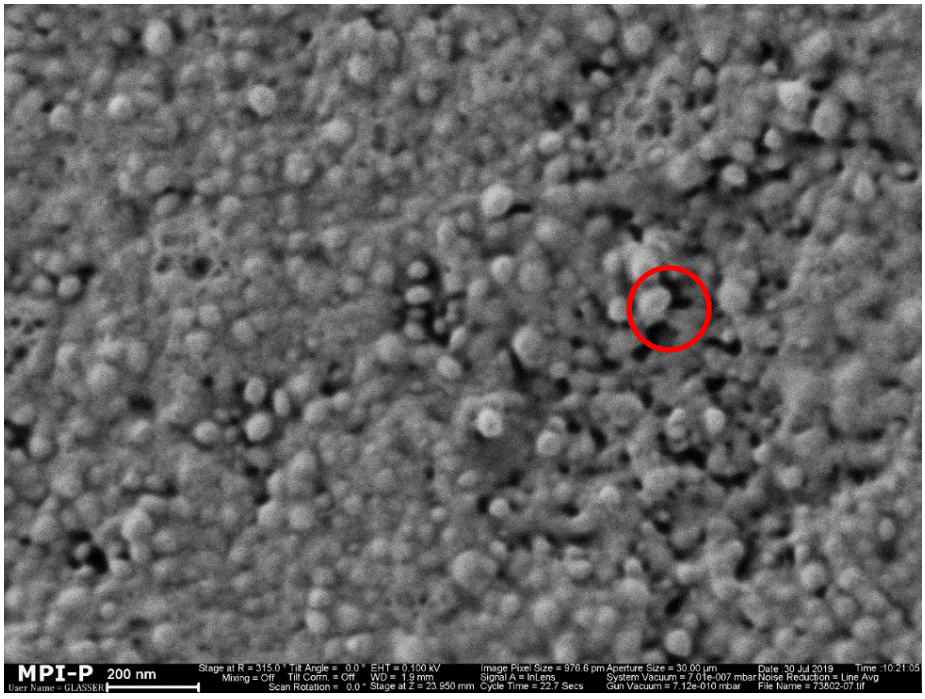

Figure 24: SEM scan of MEH-PPV/PS 1:1

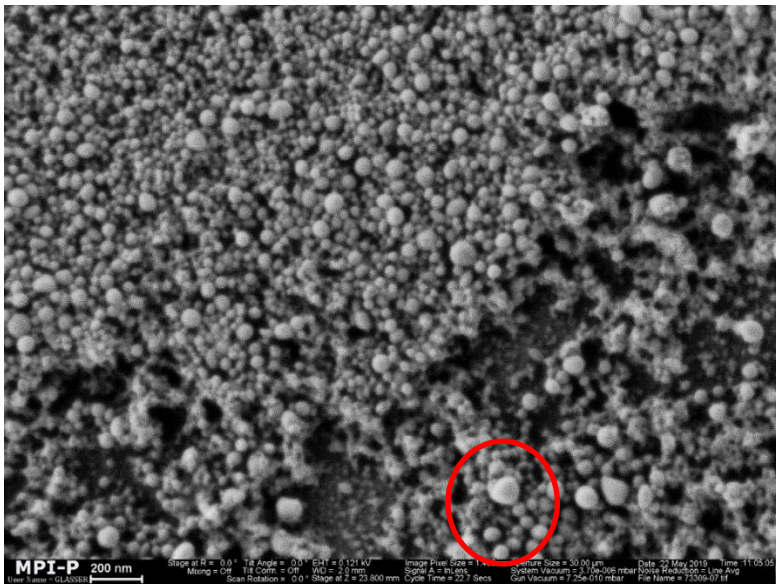

Figure 25: SEM scan of SY/PS 1:1 nanoparticles

It can be concluded effectively from SEM images that the nanoparticles formed and are spherical in shape. The images also provide evidence of a distribution of nanoparticles which is in line with the DLS results. There are also anomalies spotted as in **Figure 24: SEM scan of MEH-PPV/PS 1:1** and **Figure 25: SEM scan of SY/PS 1:1 nanoparticles** where the particles deviate from the spherical shape. This is explained by the formation of some of these particles in areas in the solution where evaporation or organic phase was un-even rate leading to distortion of the spherical shape as polymer within the micelles solidified.

4.3 Effect of surfactant and polymer concentration on size of nanoparticles

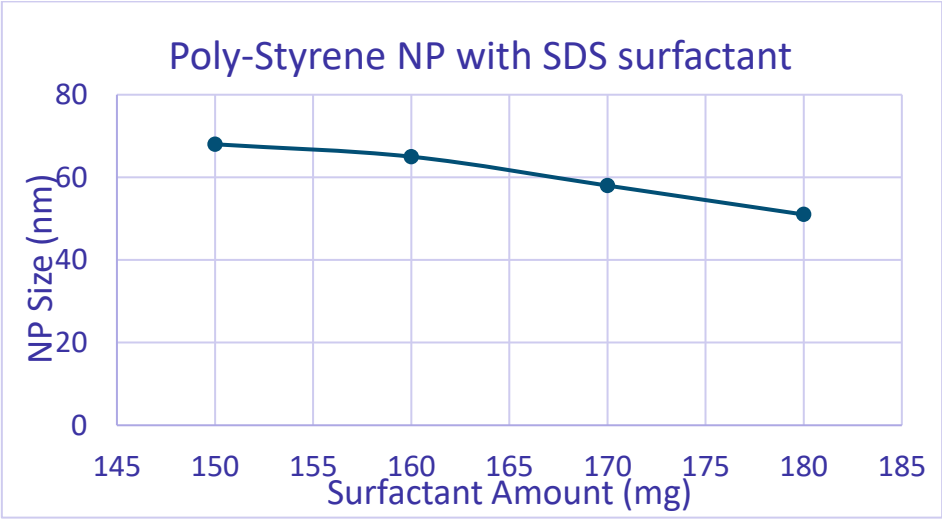

Figure 26: nanoparticle size vs surfactant concentration

It has been reported [4] that there are two main parameters to control the size of nanoparticles prepared by mini-emulsion process.

1. Increasing or decreasing the amount of surfactant in the mixture
2. Increasing or decreasing the polymer concentration

The total amount of polymer concentration was kept constant as to study the effect of blending and changing of the fraction of both semiconductor and insulator polymer in the blend. Hence, the effect of size of nanoparticles with respect to surfactant concentration was studied for our system. The findings as reported [4] were observed to be true for this system as well where increasing the surfactant concentration reduced the size of nanoparticles. This is illustrated in Figure 29 of the effect of changing surfactant amount on size of the particle during synthesis. The trend of the size reduction of nanoparticles by increasing the amount of surfactant was confirmed for this system as well. However, it was also observed that after the synthesis as surfactant amount was increased, the crystals of surfactant precipitated out in the solution. This leads to the conclusion that 150 mg of surfactant is the optimal amount where stable particles are formed and can lead to fabrication of closed nanoparticle-based films for OLEDs without wasting extra amount of surfactant.

The surface tension of the nanoparticle batches is measured after the dialysis process for each batch. This is important step to ensure that the surface tension of the aqueous particle dispersion is between the range of 57 -60 mN/m. The value for this surface tension is controlled using the dialysis time by using the data as illustrated in Table 5.

Nanoparticle Blend	Surface Tension (mN/m)
SY-PPV 1:1 PS	59.6
SY-PPV 1:3 PS	59.1
SY-PPV 1:5 PS	57.8
SY-PPV 1:9 PS	60.8
MEH-PPV 1:1 PS	57.5
MEH-PPV 1:1 PS (s)	58.5
MEH-PPV 1:1 PS (Chl)	57.5
MEH-PPV 1:3 PS	58.7
MEH-PPV 1:5 PS	60.2
PFO 1:1 PS	60.5
PFO 1:3 PS	60.5

Table 5: Surface Tension values for different polymer blends of nanoparticles

It can be concluded based on these readings that using the controlled dialysis time of 15-16h as displayed in Figure 16 helps to achieve surface tension values within the 57-60 mN/m range for nanoparticle dispersion regardless of different polymer system and is applicable to the different blends. This range of surface tension values for nanoparticle dispersion as explored before during the course of Anielen Ribeiro's PhD project are important for fabricating closed films of nanoparticles for OLEDs. The active layers of OLEDs fabricated from nanoparticle dispersions with higher or lower surface tension values from the range mentioned above lead to formation of islands due to agglomeration of particles instead of an even film.

4.4 Transmission Electron Microscopy (TEM) analysis

TEM analysis was performed to study the morphology and especially the internal morphology of the particle. The need is to understand how polymer blending works inside the particle and was any phase separation observed between the polymers or not. Nanoparticles of different blend ratios of SY-PPV/PS were prepared into thin film for analysis. The interesting case to be inspected was to be of SY-PPV 1:5 PS blend. This is because macro scale phase separation was already observed for films of pure polymer blend of this ratio. The Figure 27 and Figure 28 shows evidence of a homogenous particle as no phase separation is observed. However as the densities of both polymers are similar, the diffraction and absorption effect of electrons would be similar as well hence both polymers would appear to be similar in colour and contrast [4]. This would result in no observation of phase separation [42] even if there was any. As according to the image, the particle appears homogenous hence it can be deduced that there is no phase separation within the particle.

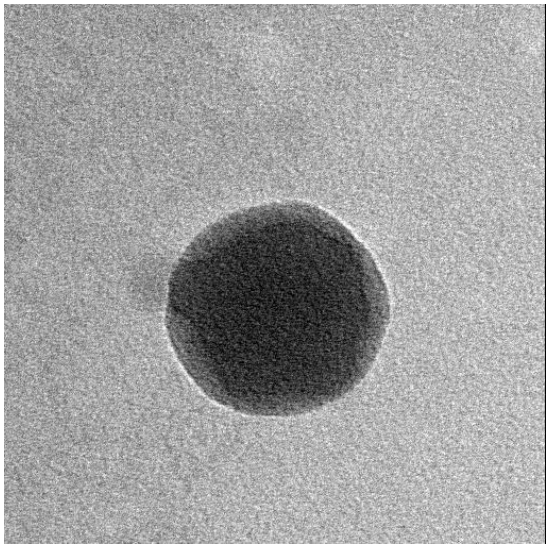

Figure 27: TEM image of SY/PS nanoparticle 1:1 blend

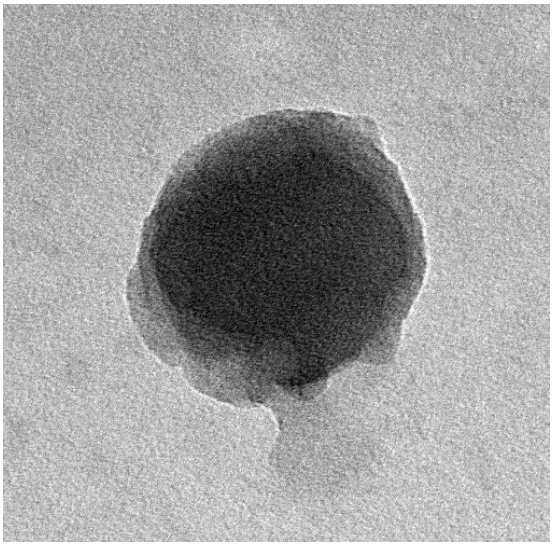

Figure 28: Another TEM scan of SY/PS nanoparticle of 1:1 blend

However, these TEM images cannot be used to be conclusively provide evidence of no phase separation within the particle. This is primarily because as both of the polymers have relatively similar density, a strong contrast difference cannot be observed with TEM. The staining of the polymers with a dye was also not possible as both

polymers are blended within the nanoparticle hence individually staining one of the polymers for example polystyrene was not practically possible.

It was thus paramount that other experimental analysis and microscopy techniques are explored to find conclusive evidence of either no phase separation or phase separation if there is any. The TEM measurements were carried out by Christoph Sieber.

4.5 DSC (Differential Scanning Calorimetry)

The DSC analysis was performed or nanoparticles of different batches to analyse the effect of blending on the glass transition temperature of the nanoparticles. [53]

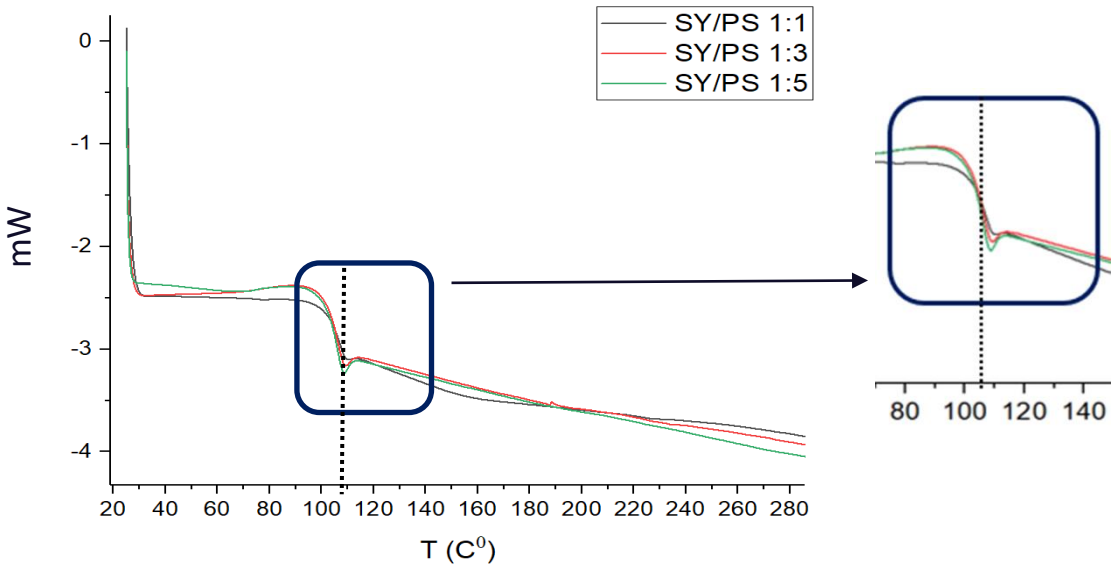

Figure 29: DSC graphs of different blends of SY/PS nanoparticles. The bump in the graph illustrates the T_g for the nanoparticle samples as observed in DSC

Figure 29 shows the analysis of the nanoparticles using DSC and the glass transition range for nanoparticles of blends of SY/PS. The glass transition temperature observed was 104°C for the blend of 1:1 of SY-PPV/PS nanoparticle sample. The values for subsequent nanoparticle blend with higher weight percentage of Polystyrene very closely overlaps with the DSC measurements of the 1:1 weight ratio nanoparticle blend. The glass transition is dominated by the presence of PS. This is due to the absence of a clear glass transition (T_g) being observed for Super-Yellow PPV [54]. These experiments were carried to understand which value to use for the annealing temperature for the nanoparticles-based films. The annealing temperature needs to be set slightly above the glass transition temperature of both polymers to ensure that the nanoparticles can coalesce into a closed film without melting away the particle itself as the idea to ensure that the polymers remain under nano-confinement to avoid phase separation on macro-scale. From the results, only one T_g is observed despite the particles having a blend of two different polymers. The observed T_g corresponds to PS. The absence of another value of glass transition temperature being observed or SY-PPV is attributed to the chemical structure

of the polymer. It has been reported [55] that it is quite difficult to determine the T_g for amorphous semi-conducing polymers [56]. This can be possibly because of the presence of both the extended conjugated system and alkyl chains in the structure and both having different temperature when they switch from glassy regime [56]. The measurements were carried out by Verona Maus.

4.6 Atomic Force Microscopy + Forced Ion Beam (AFM+FIB) analysis

These experimental analysis uses two analytical spectroscopy techniques have been applied together to study the morphology of the nanoparticles and to observe possible phase separation within the nanoparticle. The nanoparticle films of the polymers SY-PPV and PS blended in weight ratio of 1:5 within the particle, are formed on a silicon substrate using drop casting process and left to dry over-night. The films of the nanoparticles are then polished using FIB to brush away and cut through the surface of the nanoparticles in order to probe the morphology of the core of the nanoparticles. Upon the polishing of the films using FIB, AFM is used to probe the morphology of the polished area of the film.

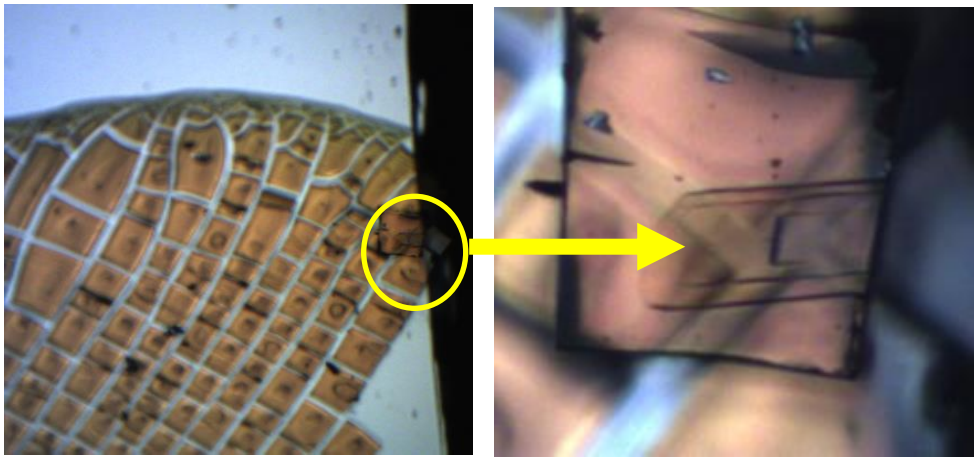

Figure 30: The figures indicate the film of nanoparticles formed by drop-casting the polymer solution. The highlighted region indicates the region of the film that was polished with FIB and where AFM cantilever is used to probe the morphology of the film

Figure 30 illustrates the polished area after FIB where the AFM cantilever will be used to probe through the film. Different modes of probing are utilized with the AFM. The tapping mode in air mode where the morphology of the sample is scanned and then the peak force mode where the tip is probed into the sample. This mode enables to check for the gradient in adhesive forces across the film and a large gradient would indicate two different phases.

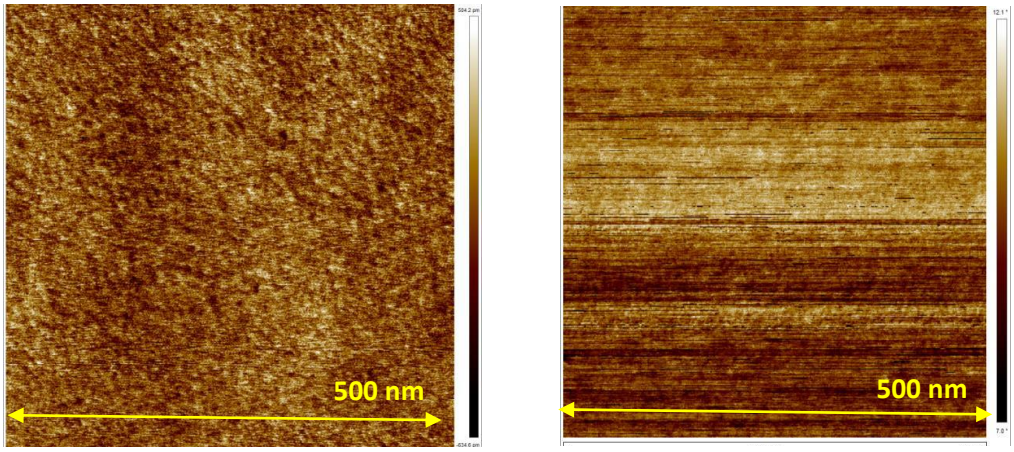

Figure 31: AFM scan using tapping mode to scan the morphology of the FIB polished area of the nanoparticle film. Scale bar = 1.3 nm for image on the left. The left image displays the topography and the phase contrast is illustrated on the right image. Scale bar 5.1 °

It is observed as demonstrated by Figure 31 using the AFM topography scan in tapping mode that no macro-scale phase separation is observed in the films of the nanoparticles. This is in stark contrast to Figure 32 which is the AFM scans of pure SY-PPV/PS 1:5 blended film where a macroscopic phase separation is clearly observed. These findings indicate and validate the hypothesis of nano-confinement of polymers helping to overcome macroscopic phase separation in the films. This has enabled to synthesize particles of different blends of polymers successfully without any phase separation being observed and closed films being formed.

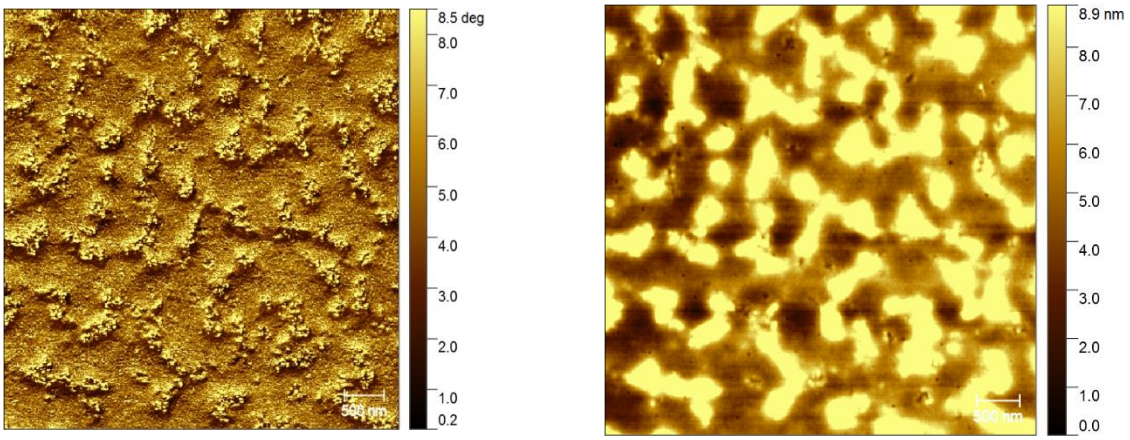

Figure 32: AFM scans of SY-PPV/PS 1:5 pure polymer blend. The contrast difference highlights the differences in height and an uneven film due to phase separation of the two polymers.

The AFM scans in Figure 33 show the results of the AFM probing mode in order to test the adhesiveness of the surface. The topography of the scan displays no macroscopic phase separation. The image on the right displays the adhesiveness scan which also despite not being fully homogenous displays no prominent region with strongly different adhesive forces. It is also interesting to note that the image length scale is 500 nm and as the average size of nanoparticles is approximately 70 nm, this length scale would already contain several nanoparticles. For large portion of the image, the area is homogenous indicating just one phase despite several nanoparticles being scanned in that length scale. This can be further used to conclude that the polymers are well blended within the confines of the nanoparticle.

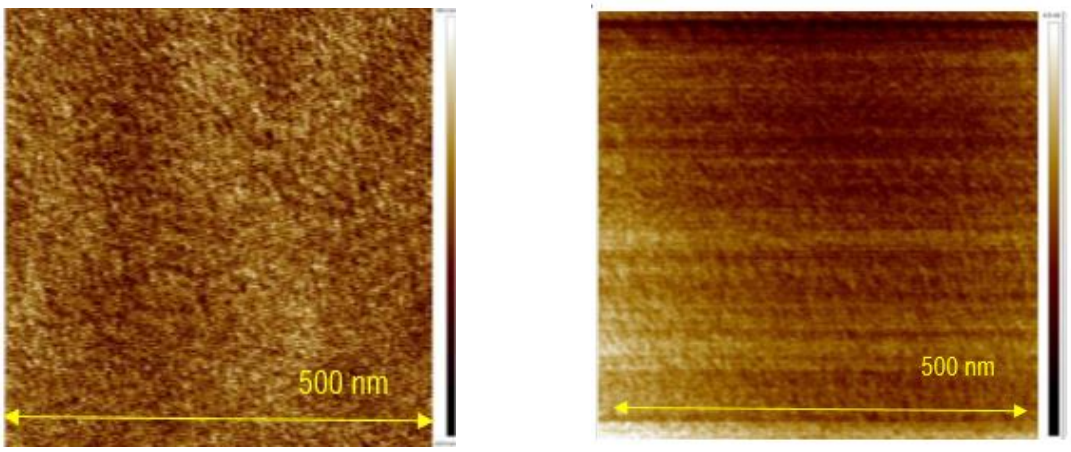

Figure 33: Scale bar 1.1 nm for the image on the left which represents the AFM image of the topography using peak force AFM. Scale bar 3.4 nN for the image on the right which illustrates the adhesion map of the sample.

It can be conclusively stated that blending the two polymers under nano-confinement has enabled to overcome macro-phase separation for a blend of SY-PPV and PS blend in a weight ratio of 1:5 as macro phase separation has previously been observed already for a pure blended film of these two polymers in the very same weight ratio.

4.7 XPS analysis

The XPS analysis was also performed for nanoparticle blends to study the phase blending within the nanoparticle. Generally, SEM and TEM is used as a preferred method to study the structure within the nanoparticles. However in the case of no strong contrast difference which was observed for this system, TEM and SEM don't provide sufficient information [46]. XPS is thus used to probe the structure of the nanoparticle.

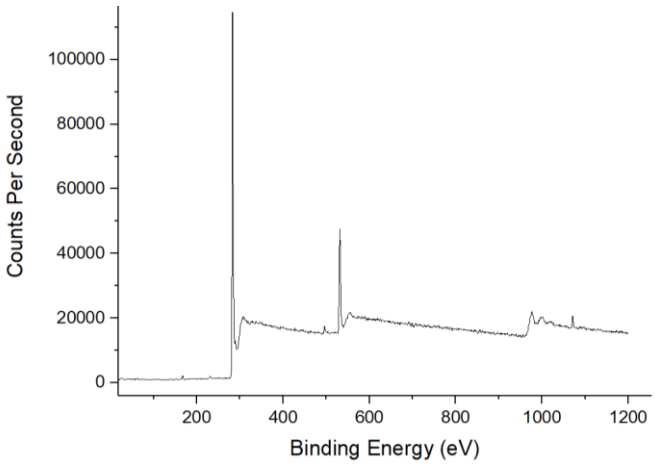

Figure 34: XPS graph of SY/PS 1:5 weight ratio blended nanoparticle sample illustrating the binding energy levels as measured for the different elements in the nanoparticle sample

Figure 34 displays the XPS spectrum for the entire sample of a SY/PS 1:5 nanoparticle blend. The peaks illustrates the binding energies and correspond to certain bond lengths of specific elements.[57, 58] This will enable to identify which elements exist in the top most layer of the nanoparticles which will in turn help predict the presence of certain polymer in the outermost layer. [46] The analysis also helps in predicting the internal morphology of the sample. In case for example, the outermost layer scanned by XPS has no signal from bonds from elements present in polystyrene and only from SDS and SY-PPV, then a core-shell morphology can be predicted. [58]

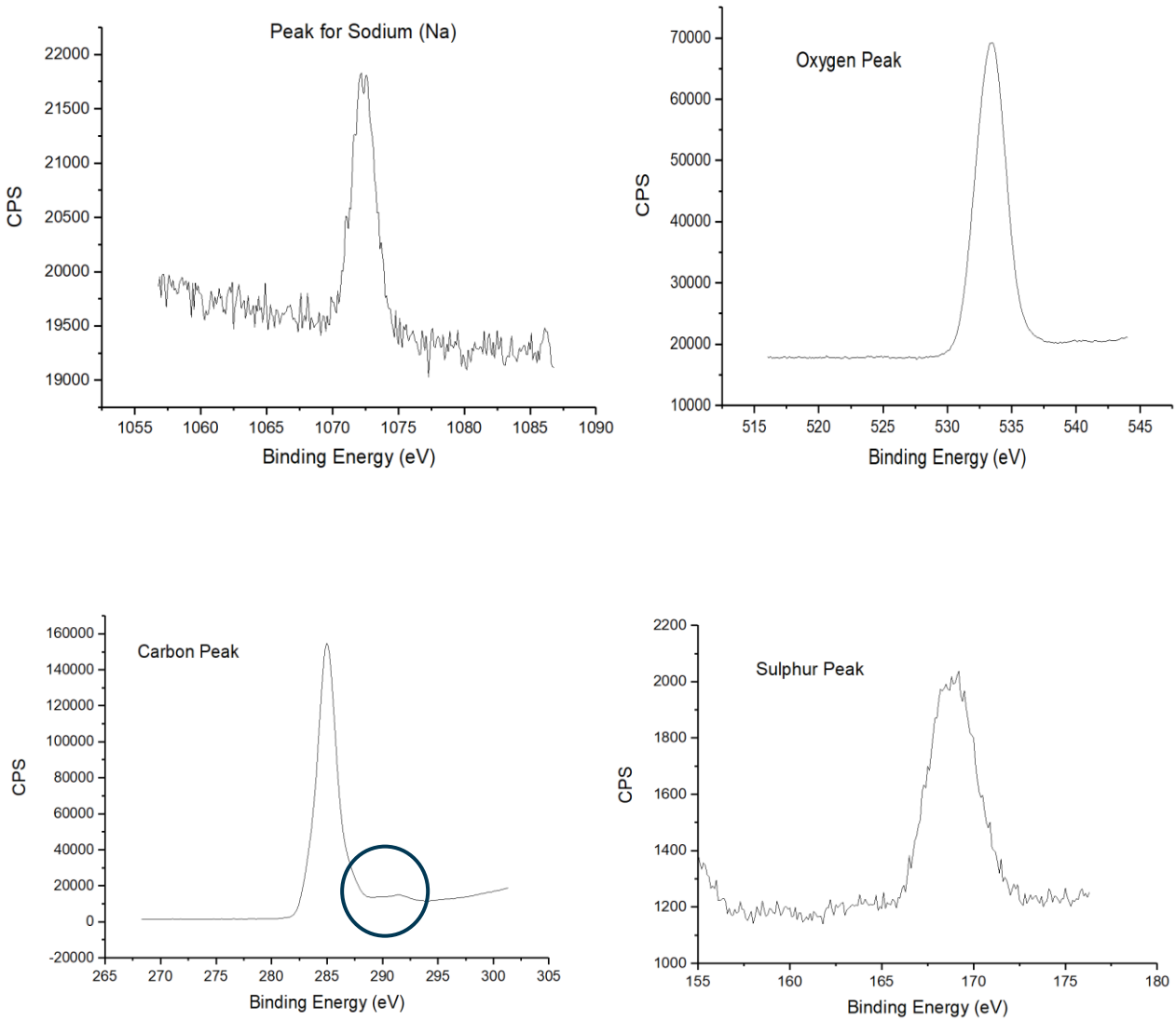

Figure 35: The graphs illustrates the peaks for the elements observed during the XPS scans of the SY/PS 1:5 blended nanoparticle.

The Figure 35 represents binding energies for different elements observed during the XPS scans of the SY/PS 1:5 samples. Carbon, Oxygen, Sulphur and Sodium is detected. The peaks from Sodium and Sulphur represents the presence of SDS as the head group contains Sodium and Sulphur atoms. The peak from carbon can be representative of SDS, SY as well as polystyrene because of presence of Carbon and Hydrogen bond in all three polymers. Ideally a difference in chemical environment [46] causes a shift in peak of the XPS spectra, however

no such major shift in peaks is observed. This can be observed with a very minor shift in the Carbon-Hydrogen peak with a shoulder next to the main peak indicating for possibly bonds with different chemical environments in different chemical compounds as the peaks could overlap considerably. The shoulder would indicate the signal from chemically shifted Carbon-Hydrogen bond in the conjugated carbon bond system present in both Polystyrene and SY-PPV. The other possible explanation is that only signals from SDS is detected as it forms a thicker shell than expected and no signals are recovered from SY or PS polymers. However, the presence of all strong peaks and a shoulder at the carbon end indicate presence of detection of different Carbon and Hydrogen bonds from different polymers. The XPS results displayed these interesting characteristics, however the present results cannot be used to conclusively conclude for evidence of no phase separation within the nanoparticle. This could be because of several peaks from different chemical bonds not displaying a prominent chemical shift despite being in different chemical environment and thus overlapping each other. This would mask the presence of different peaks which would not appear in the spectrum.

XPS results enable to better understand the morphology of the nanoparticles. The signals from the Sodium and Sulphur indicate the presence of an SDS shell around the polymeric nanoparticle. The exact thickness of the shell cannot be determined using XPS, however the presence of the shoulder on the Carbon peak indicates the detection of signal from the polymers. This would mean the shell is less than 10 nm thick as the XPS measures surface signals to a maximum depth of 10 nm. It can be concluded that the presence of signal of Carbon and Hydrogen from conjugated pi orbital system can be from both SY-PPV and PS polymers, however, no evidence from the spectra is available to differentiate and highlight the presence of any one of these polymers.

4.8 OLEDs device performance and efficiency

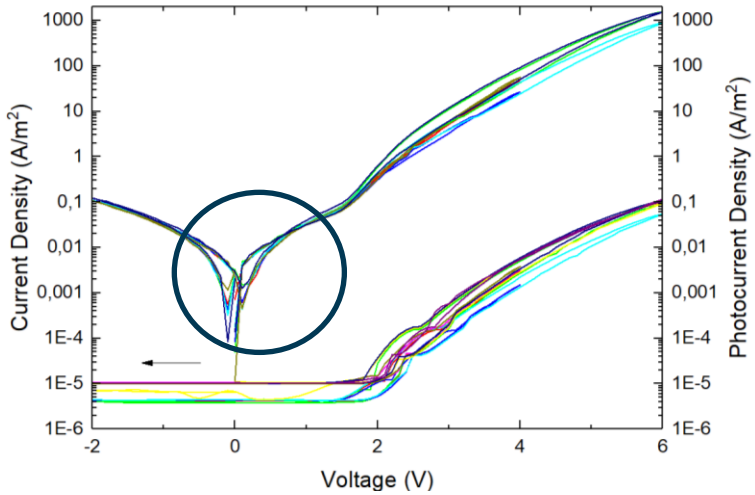

Figure 36: Current vs Voltage plot for a 2-layered device of MEH-PPV/PS 1:1 nanoparticle blend. The highlighted region indicated the leakage current regime.

The long-term project scope involves improving the efficiency of the OLED devices and to find a method to fabricate novel OLED devices from water-based polymer dispersions. The OLEDs are fabricated as highlighted by the procedure in section 2.4. During the OLED fabrication process, different attempts were made to improve the charge transport and efficiency of the devices. The charge transport is observed using Current-

Voltage curves (JV curves) as shown in Figure 36. The first part of the curve as highlighted by the circle in Figure 36 illustrates the regime of leakage current flow. It is important for the devices to have low amount of leakage current. Leakage current arises due to an uneven formation of the film which can lead to electrons diffusing and migrating directly from the cathode to the anode without wholly passing through the semi-conductor polymer film. This is unwanted as leakage current leads to non-radiative emission and is loss process which will decrease the efficiency of the OLED device. Figure 39 shows a device with high leakage current. One can notice the different in leakage current amount to the device in Fig. 36 and then the corresponding efficiencies in Figure 37 and Figure 40. The device with high leakage current shows markedly lower current efficiency. Although the efficiency of the OLED is not solely dependent on the amount of leakage current as other factors also contribute such as cathode quenching, light out-coupling, but it is certainly a factor which influences the efficiency of the devices. It has been observed that a double spin-coated nanoparticle active layer device provides lower amount of leakage current while still ensuring a closed film formation without a short circuit. The two layered devices have also demonstrated higher efficiencies as compared to a three-layered device. This can be observed in Fig 37 and 38 which are comparative plots for a two-layered device and a three-layered device. The additional benefit of fabricating devices with 2-layers instead of 3-layers of nanoparticles is the utilization of lesser amount of polymer material.

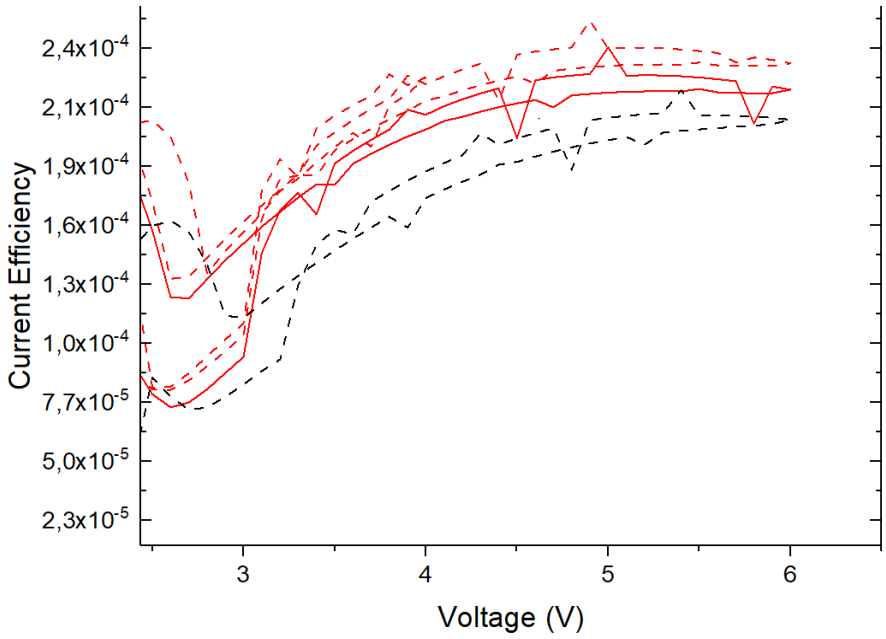

Figure 37: MEH-PPV/PS 1:1 2-layered nanoparticle device efficiency curves. The thickness of the device as measured is 125 nm.

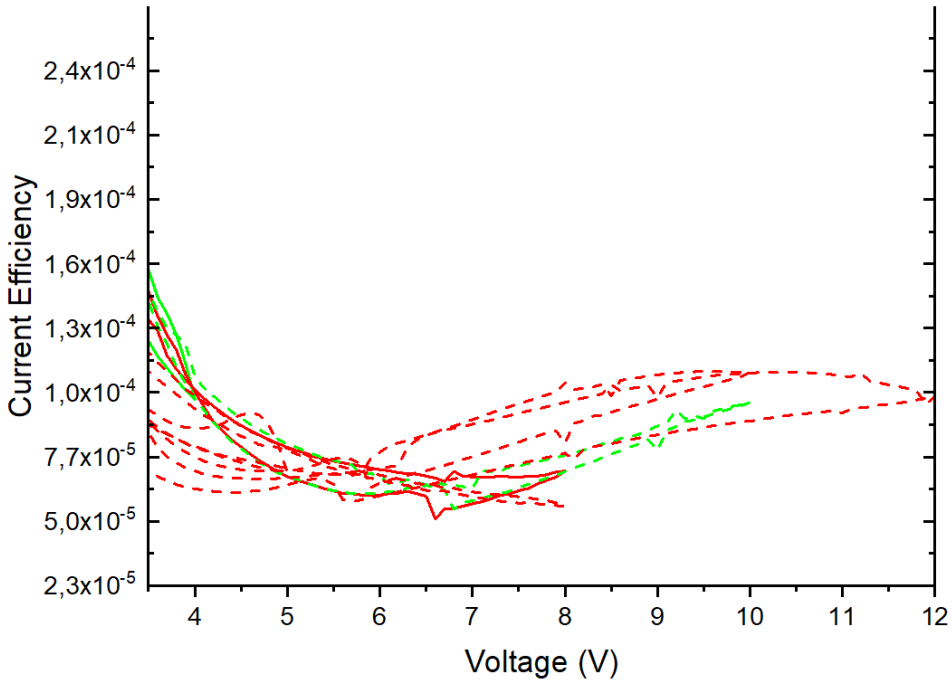

Figure 38: MEH-PPV/PS 1:1 3-layered nanoparticle device efficiency curves. The thickness of the device as measured is 165 nm.

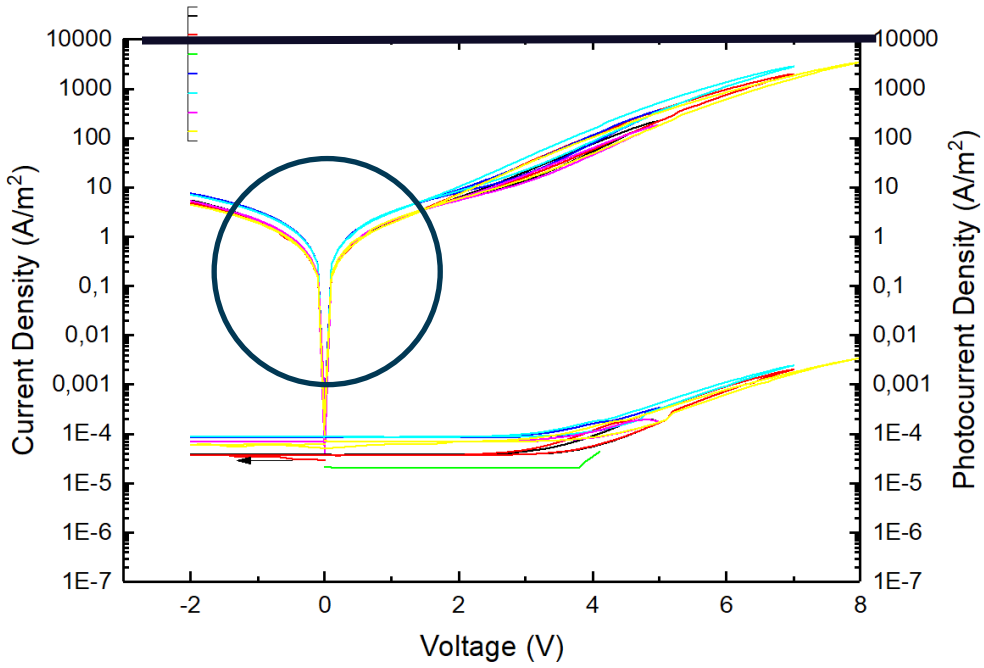

Figure 39: MEH-PPV/PS 1:1 blended nanoparticle device with high leakage current. The encircle region highlights the region of device with leakage current regime.

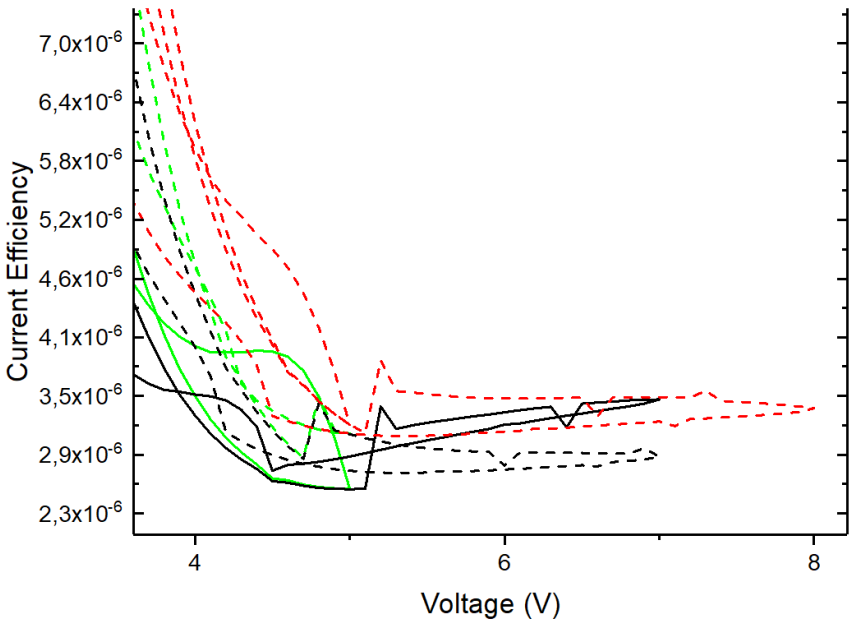

Figure 40: Current Efficiency graph for the corresponding MEH-PPV/PS 1:1 nanoparticle device of which the Current-Voltage curves are illustrated in Figure 42

The efficiencies of the nanoparticle-based devices have been adjusted to account for the loss in transmission of light due to the comparative opaque nature of the Gold anode. **Figure 41** illustrates the transmission spectrum for Gold spectrum. The measurements were done by Anielen Ribeiro and used as it is. Using the transmission spectrum, 30% transmission value was approximated and used from the graph as a standard value for all device measurements. The loss of 70% was adjusted consequently in the current efficiency calculations.

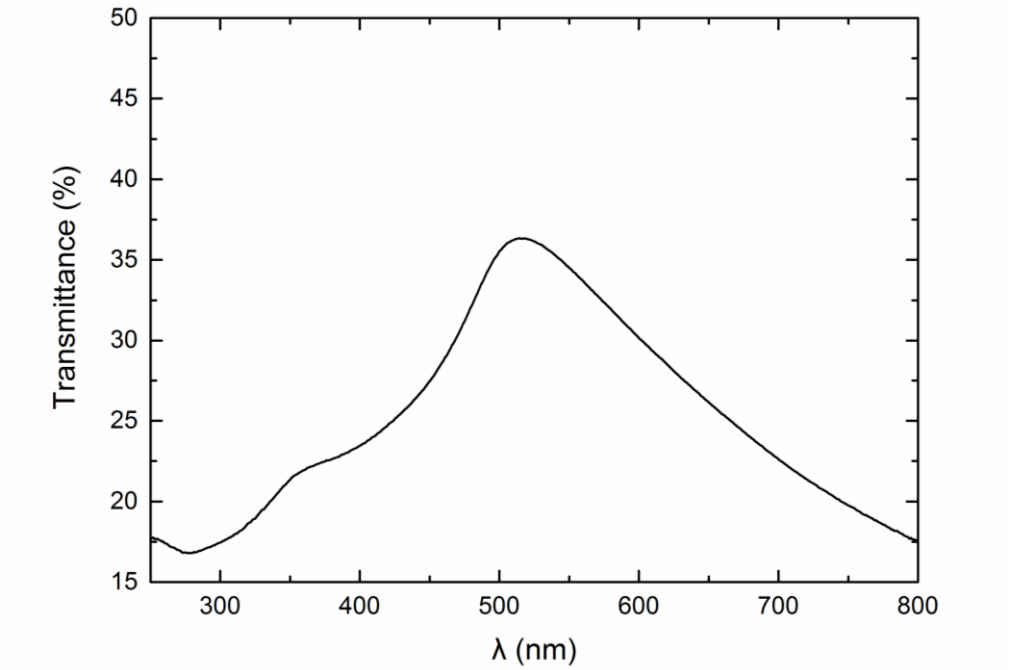

Figure 41: Transmission spectra of 20 nanometer thick gold layer indicating percentage transmission of light through Gold layer.

The OLED devices were fabricated using blends of different polymers and a comparative analysis displays that MEH-PPV based devices provided higher current efficiencies and performed better than PFO based or SY-PPV based devices. Error! Reference source not found. illustrates the performance of a PFO/PS 1:1 device. The leakage current for this device is higher as shown by the highlighted region in Figure 42. This stems from PFO having lower efficiency as a semi-conductor polymer compared to MEH-PPV which has better efficiency. The hysteresis observed in the PFO devices is due to the hole injection barrier posed by the HOMO of the PFO. However, the hysteresis is reduced in repeated scans as once the charged is built up as in the secondary and tertiary scans, the injection barrier is not present anymore and hence the hysteresis is only observed during the first scan.

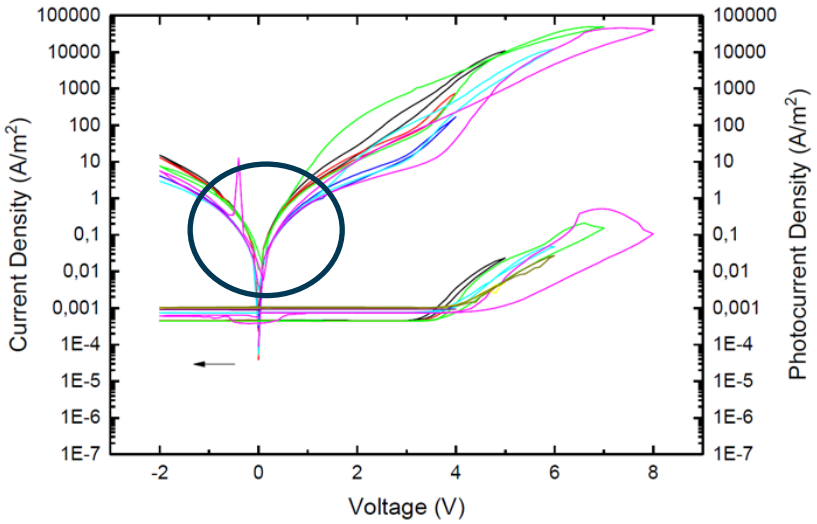

Figure 42: JV curves for PFO/PS 1:1 OLED device. The highlight region illustrates the leakage current or the device

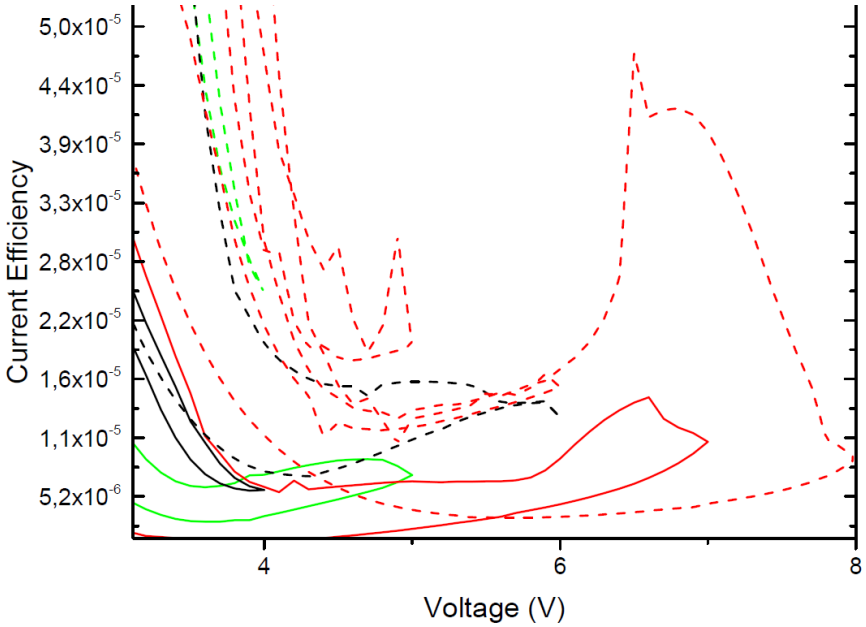

Figure 43: Current efficiency plot for OLEDs fabricated from PFO/PS 1:1 blended nanoparticle films.

The better performance of the MEH-PPV/PS nanoparticles films-based devices is possibly because of MEH-PPV having low turn on voltage. The effect of using Toluene during the synthesis of nanoparticles would also allow for better alignment of the conjugated segments of the polymer chains as the solvent shows better affinity with the polymer. This would enable and efficient hopping transport of charges and better recombination and eventually higher efficiencies. However, the exact effect of use of different organic solvents during nanoparticle synthesis on OLED performance and particle structure is out of the research scope of the project and hence no been studied in detail.

5- Conclusions

The thesis project's primary objectives were to attempt to explore the synthesis of nanoparticles of different polymer blends to overcome macroscopic phase separation and synthesize polymer layers for OLEDs using environmentally friendly solvents. It was also then important to study the effect of nanoparticle blending in different ratios on device performance. The nanoparticle synthesis was successfully achieved with nanoparticles formed from blends of different semiconducting polymers with an insulator. Mini-emulsion method and recipe of controlled polymer and surfactant concentration of 2.5% volume percent polymer in organic phase and 1.5% volume percent of surfactant in aqueous phase has enabled to synthesize stable nanoparticle dispersions for three different polymer systems, namely; SY-PPV:PS, MEH-PPV: PS and PFO:PS. The internal morphology of the particles as probed using FIB and AFM revealed that the idea behind the use of nanoparticles as hypothesized was to overcome macroscopic phase separation for polymer blends using nano-confinement, has been achieved. This was visualized and successfully proven with AFM and FIB measurements for SY/PS 1:5 blended nanoparticles. The morphology of the nanoparticles for all three systems of semiconductor and insulating blends has appeared to be spherical by visualizations from TEM and SEM with spread in sizes of the particles observed using SEM and DLS measurements. The spread of the population nanoparticles of MEH-PPV and SY-PPV can also be visualized in the SEM scans. SY-PPV/PS blended particles also displayed interesting trend of reduction in average size of the nanoparticle dispersion as the weight ratio of the two polymers was altered. The amount of polystyrene was increased by weigh ratio from 1:1 to 1:3, 1:5 and 1:9. A similar trend was not observed for the two other semiconductor/insulator nanoparticle blends. TEM was also deployed to study the blending of SY-PPV/PS polymer within the nanoparticles. Due to the similar density of both polymers, the contrast between the two polymers in a TEM image is very similar. TEM images only revealed one homogeneous particle. This could indicate very good blending within the nanoparticle as well or could also be due to the lack of contrast hence TEM cannot be used to conclusively state either effect and hence was not deployed consequently for the remaining blended systems of MEH-PPV and PFO because of similar reasons.

XPS resolved elemental spectra has given information of the thickness of SDS shell as well as possible evidence of well blended homogenous phase for SY-PPV/PS 1:5 blended nanoparticles. It has shown initial promise of being another tool to probe the internal morphology of the nanoparticles to better understand mixing and can be used to study the morphology using different blends of polymers. However current evidence of XPS spectra is insufficient for this concrete proof of a well-blended semiconductor and insulator polymer phase. DSC analysis of the polymeric nanoparticle blends of SY-PPV/PS in different ratios displayed only a single glass transition temperature. The glass transition temperature observed was 104°C for the blend of 1:1 of SY-PPV/PS and 1°C higher for subsequent blends with higher weigh percentage of Polystyrene. There is no glass transition observed for SY-PPV hence DSC is not able to provide insights into blend morphology for SY-PPV/PS blended nanoparticles and was not pursued further for analysis of consequent systems of MEH-PPV and PFO.

OLED devices have been successfully fabricated using layers of polymeric nanoparticles from aqueous dispersion and free of halogenated solvents. The devices fabricated with spin-coated two layered nanoparticle-based films have shown lower leakage current and higher efficiencies and could be set as the norm for further exploration work for device fabrication using nanoparticle blends. The concentration of

surfactant is controlled by using values of surface tension and to be kept in the range of 57-60 mN/m. Of the two semi-conductor-based polymer systems compared, namely; MEH-PPV/PS and PFO/PS based active layer OLEDs, the MEH-PPV/PS based devices have shown higher efficiencies approaching values of $2.2x10^{-4}$ as compared to efficiencies of $3.8x10^{-5}$for PFO/PS based devices.

It will be interesting in the future to further look into the effect of using different organic solvents to synthesize nanoparticles and its effect on OLED device performance. As different organic solvents have different chemical affinity with the different semi-conducting polymers used, the blending within the nanoparticle and consequent device performance would be possibly altered. It will be interesting to study this effect in future research work. Another interesting area of subsequent research would be the measurement of light outcoupling efficiency of nanoparticle based films and pure blended films and how to subsequently improve the light outcoupling for nanoparticle based films.

Acknowledgements

I would like to thank Dr. Jasper Michels for his supervision and for his support. I would also like to thank Anielen Halda Ribeiro for her personal coaching and support during experimental process and the project. I thoroughly enjoyed my time at MPIP where I learned a lot with theoretical and practical training. I would also like to thank Professor Rolf Mülhaupt for his support and advice during the thesis and for University of Freiburg/University of Strasbourg for the academic knowledge transfer and for the academic learnings during the course of the Master's program. I would also like to thank Professor Paul Blom and the research group for the academic knowledge and experimental guidance during the course of thesis. Lastly I would like to thank my family, especially my mother, and my close friends for that unwavering support and encouragement, it wouldn't be possible without them!

References

1. Chiang, C.K., et al., *Electrical Conductivity in Doped Polyacetylene.* Physical Review Letters, 1977. 39(17): p. 1098-1101.
2. Abbaszadeh, D., et al., *Elimination of charge carrier trapping in diluted semiconductors.* Nature Materials, 2016. 15: p. 628.
3. Landfester, K., *The Generation of Nanoparticles in Miniemulsions.* Advanced Materials, 2001. 13(10): p. 765-768.
4. Colberts, F.J.M., M.M. Wienk, and R.A.J. Janssen, *Aqueous Nanoparticle Polymer Solar Cells: Effects of Surfactant Concentration and Processing on Device Performance.* ACS Applied Materials & Interfaces, 2017. 9(15): p. 13380-13389.
5. Bardsley, J.N., *International OLED technology roadmap.* IEEE Journal of Selected Topics in Quantum Electronics, 2004. 10(1): p. 3-9.
6. Forrest, S., P. Burrows, and M. Thompson, *The dawn of organic electronics.* IEEE spectrum, 2000. 37(8): p. 29-34.
7. Chai, Z., et al., *Tailorable and Wearable Textile Devices for Solar Energy Harvesting and Simultaneous Storage.* ACS Nano, 2016. 10(10): p. 9201.
8. Yu, G., et al., *Polymer Photovoltaic Cells: Enhanced Efficiencies via a Network of Internal Donor-Acceptor Heterojunctions.* Science, 1995. 270(5243): p. 1789-1791.
9. D'Olieslaeger, L., et al., *Eco-Friendly Fabrication of PBDTTPD:PC71BM Solar Cells Reaching a PCE of 3.8% Using Water-Based Nanoparticle Dispersions.* Org. Electron., 2017. 42: p. 42.
10. Lee, J.Y., J.H. Kwon, and H.K. Chung, *High efficiency and low power consumption in active matrix organic light emitting diodes.* Organic Electronics, 2003. 4(2): p. 143-148.
11. Musyanovych, A., et al., *Preparation of Biodegradable Polymer Nanoparticles by Miniemulsion Technique and Their Cell Interactions.* Macromolecular Bioscience, 2008. 8(2): p. 127-139.
12. Kietzke, T., et al., *Novel approaches to polymer blends based on polymer nanoparticles.* Nature Materials, 2003. 2(6): p. 408-412.
13. Kunz, A., P.W.M. Blom, and J.J. Michels, *Charge carrier trapping controlled by polymer blend phase dynamics.* Journal of Materials Chemistry C, 2017. 5(12): p. 3042-3048.
14. Nicolai, H.T., et al., *Unification of trap-limited electron transport in semiconducting polymers.* Nature Materials, 2012. 11(10): p. 882-887.
15. Brabec, C.J., N.S. Sariciftci, and J.C. Hummelen, *Plastic Solar Cells.* Advanced Functional Materials, 2001. 11(1): p. 15-26.
16. Bag, M., et al., *Fabrication Conditions for Efficient Organic Photovoltaic Cells from Aqueous Dispersions of Nanoparticles.* RSC Adv., 2014. 4(85): p. 45325.
17. Li, L. and H. Kosina, *Charge Transport in Organic Semiconductor Devices*. 1970. p. 301-323.
18. Blom, P.W.M. and M.C.J.M. Vissenberg, *Charge transport in poly(p-phenylene vinylene) light-emitting diodes.* Materials Science and Engineering: R: Reports, 2000. 27(3): p. 53-94.
19. Friend, R.H., et al., *Electroluminescence in conjugated polymers.* Nature, 1999. 397(6715): p. 121-128.
20. Miller, A. and E. Abrahams, *Impurity Conduction at Low Concentrations.* Physical Review, 1960. 120(3): p. 745-755.

21. **Pasveer, W.F., et al., *Unified Description of Charge-Carrier Mobilities in Disordered Semiconducting Polymers.* Physical Review Letters, 2005. 94(20): p. 206601.**
22. **Arkhipov, V., et al., *Charge carrier mobility in doped semiconducting polymers.* Applied Physics Letters, 2003. 82(19): p. 3245-3247.**
23. **Favre, E., et al., *Application of Flory-Huggins theory to ternary polymer-solvents equilibria: A case study.* European Polymer Journal, 1996. 32(3): p. 303-309.**
24. **in *Intermolecular and Surface Forces (Third Edition)*, J.N. Israelachvili, Editor. 2011, Academic Press: San Diego. p. 635-660.**
25. **Pirika. *Surfactant and Hansen Solubility Parameter (HSP)*. 2013. January 29; Available from: https://pirika.com/NewHP/PirikaE2/Surfactant.html.**
26. **Marshall, C.E., *"Theory of the stability of lyophobic colloids. The interaction of particles having an electric double layer." E. J. W. Verwey and J. T. G. Overbeek, with the collaboration of K. van Ness. Elsevier, New York-Amsterdam, 1948, 216 pp., $4.50.* Journal of Polymer Science, 1949. 4(3): p. 413-414.**
27. **Dzyaloshinskii, I.E.e., et al., *The general theory of van der Waals forces*, in *Perspectives in Theoretical Physics*. 1992, Elsevier. p. 443-492.**
28. **Hamaker, H.C., *The London—van der Waals attraction between spherical particles.* physica, 1937. 4(10): p. 1058-1072.**
29. **Okubo, T., *Extraordinary behavior in the structural properties of colloidal macroions in deionized suspension and the importance of the Debye screening length.* Accounts of Chemical Research, 1988. 21(7): p. 281-286.**
30. **Derjaguin, B. and L. Landau, *Theory of the stability of strongly charged lyophobic sols and of the adhesion of strongly charged particles in solutions of electrolytes.* Progress in Surface Science, 1993. 43(1): p. 30-59.**
31. **Scott, J.C., et al., *Charge transport processes in organic light-emitting devices.* Synthetic Metals, 2000. 111-112: p. 289-293.**
32. **Sirringhaus, H., et al., *High-resolution inkjet printing of all-polymer transistor circuits.* Science, 2000. 290(5499): p. 2123-2126.**
33. **Moiz, S.A., et al., *Space charge-limited current model for polymers.* Conducting Polymers, 2016: p. 91.**
34. **Blom, P.W. and M.J. De Jong, *Electrical characterization of polymer light-emitting diodes.* IEEE Journal of selected topics in quantum electronics, 1998. 4(1): p. 105-112.**
35. **Wetzelaer, G.A.H., et al., *Trap-assisted and Langevin-type recombination in organic light-emitting diodes.* Physical Review B, 2011. 83(16): p. 165204.**
36. **Lang, N.D. and W. Kohn, *Theory of Metal Surfaces: Work Function.* Physical Review B, 1971. 3(4): p. 1215-1223.**
37. **Lara Bullejos, P., et al., *Unified model for the injection and transport of charge in organic diodes.* Journal of Applied Physics, 2008. 103(6): p. 064504.**
38. **Chandra, W., et al., *Two-dimensional analytical Mott-Gurney law for a trap-filled solid.* Applied physics letters, 2007. 90(15): p. 153505.**
39. **Shockley, W. and W.T. Read, *Statistics of the Recombinations of Holes and Electrons.* Physical Review, 1952. 87(5): p. 835-842.**
40. **Mark, P. and W. Helfrich, *Space‐charge‐limited currents in organic crystals.* Journal of Applied Physics, 1962. 33(1): p. 205-215.**

41. Abbaszadeh, D., et al., *Electron Trapping in Conjugated Polymers.* Chemistry of Materials, 2019. 31(17): p. 6380-6386.
42. Workman Jr, J.J., *Concise Handbook Of Analytical Spectroscopy, The: Theory, Applications, And Reference Materials (In 5 Volumes)*. 2016: World Scientific.
43. Donald, A.M., *The use of environmental scanning electron microscopy for imaging wet and insulating materials.* Nature Materials, 2003. 2(8): p. 511-516.
44. McClelland, G.M., R. Erlandsson, and S. Chiang. *Atomic Force Microscopy: General Principles and a New Implementation*. 1987. Boston, MA: Springer US.
45. Giannuzzi, L.A., *Introduction to focused ion beams: instrumentation, theory, techniques and practice*. 2004: Springer Science & Business Media.
46. Sarma, D.D., et al., *X-ray Photoelectron Spectroscopy: A Unique Tool To Determine the Internal Heterostructure of Nanoparticles.* Chem. Mater., 2013. 25: p. 1222.
47. Sharifi Dehsari, H., et al., *Effect of precursor concentration on size evolution of iron oxide nanoparticles.* CrystEngComm, 2017. 19(44): p. 6694-6702.
48. Marks, M., et al., *Building intermixed donor–acceptor architectures for water-processable organic photovoltaics.* Physical Chemistry Chemical Physics, 2019. 21(10): p. 5705-5715.
49. D'Olieslaeger, L., et al., *Tuning of PCDTBT:PC71BM blend nanoparticles for eco-friendly processing of polymer solar cells.* Solar Energy Materials and Solar Cells, 2017. 159: p. 179-188.
50. Nguyen, T.-Q. and B.J. Schwartz, *Ionomeric control of interchain interactions, morphology, and the electronic properties of conjugated polymer solutions and films.* The Journal of Chemical Physics, 2002. 116(18): p. 8198-8208.
51. Nguyen, T.-Q., V. Doan, and B.J. Schwartz, *Conjugated polymer aggregates in solution: Control of interchain interactions.* The Journal of Chemical Physics, 1999. 110(8): p. 4068-4078.
52. Burns, S., et al., *Effect of thermal annealing Super Yellow emissive layer on efficiency of OLEDs.* Scientific Reports, 2017. 7(1): p. 40805.
53. Zhang, C., Y. Guo, and R.D. Priestley, *Glass Transition Temperature of Polymer Nanoparticles under Soft and Hard Confinement.* Macromolecules, 2011. 44(10): p. 4001-4006.
54. Christie, D., et al., *Glass transition temperature of colloidal polystyrene dispersed in various liquids.* Journal of Polymer Science Part B: Polymer Physics, 2016. 54(17): p. 1776-1783.
55. Sharma, A., et al., *Probing the Relationship between Molecular Structures, Thermal Transitions, and Morphology in Polymer Semiconductors Using a Woven Glass-Mesh-Based DMTA Technique.* Chemistry of Materials, 2019. 31(17): p. 6740-6749.
56. Xie, R., et al., *Glass Transition Temperature of Conjugated Polymers by Oscillatory Shear Rheometry.* Macromolecules, 2017. 50(13): p. 5146-5154.
57. Sublemontier, O., et al., *X-ray Photoelectron Spectroscopy of Isolated Nanoparticles.* The Journal of Physical Chemistry Letters, 2014. 5(19): p. 3399-3403.
58. Bernardi, F., et al., *Unraveling the Formation of Core–Shell Structures in Nanoparticles by S-XPS.* J. Phys. Chem. Lett., 2010. 1: p. 912.